MIMO Equalization for Space Division Multiplexing in Optical Communications

Author:	Saumya Jha
Degree Programme:	Electrical Engineering and Information Technology
Examiner:	Prof. Dr. rer. nat. Sascha Preu
Department:	Institute for Microwave Engineering and Photonics
Supervisor:	Juan L. Moreno Morrone, Irene Rodriguez Lamoso
Start Date:	01.03.2023
Date Of Submission:	29.08.2023
Examination Date:	29.08.2023
Master thesis	(18-20-5000, WiSe 2022/23)

TECHNISCHE UNIVERSITÄT DARMSTADT

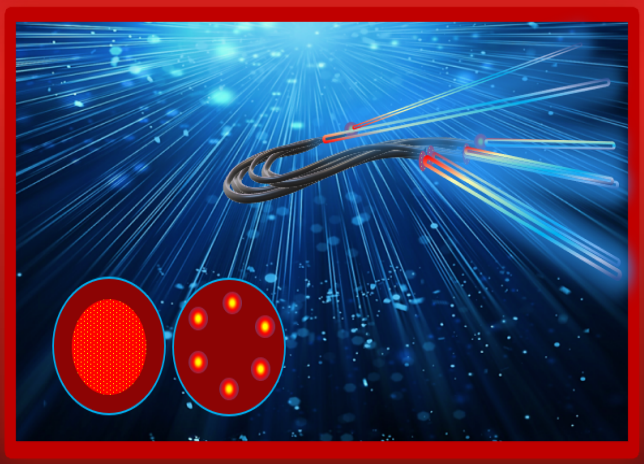

Topic: MIMO Equalization for Space Division Multiplexing in Optical Communications

Affidavit/Eidesstattliche Versicherung

Erklärung zur Abschlussarbeit gemäß §22 Abs. 7 und §23 Abs. 7 APB TU Darmstadt.
Hiermit versichere ich, Saumya Jha, vorliegende Master-Thesis / Bachelor-Thesis gemäß §22 Abs. 7 APB der TU Darmstadt ohne Hilfe Dritter und nur mit den angegebenen Quellen und Hilfsmitteln angefertigt zu haben. Alle Stellen, die Quellen entnommen wurden, sind als solche kenntlich gemacht worden. Diese Arbeit hat in gleicher oder ähnlicher Form noch keiner Prüfungsbehörde vorgelegen. Mir ist bekannt, dass im Falle eines Plagiats (§38 Abs.2 APB) ein Täuschungsversuch vorliegt, der dazu führt, dass die Arbeit mit 5,0 bewertet und damit ein Prüfungsversuch verbraucht wird. Abschlussarbeiten dürfen nur einmal wiederholt werden. Bei der abgegebenen Thesis stimmen die schriftliche und die zur Archivierung eingereichte elektronische Fassung gemäß §23 Abs. 7 APB überein.

English translation for information purposes only:
Thesis Statement pursuant to §22 paragraph 7 and §23 paragraph 7 of APB TU Darmstadt I, Saumya Jha, herewith formally declare that I, Saumya Jha, have written the submitted thesis independently pursuant to §22 paragraph 7 of APB TU Darmstadt. I did not use any outside support except for the quoted literature and other sources mentioned in the paper. I clearly marked and separately listed all of the literature and all of the other sources which I employed when producing this academic work, either literally or in content. This thesis has not been handed in or published before in the same or similar form. I am aware, that in case of an attempt at deception based on plagiarism (§38 Abs. 2 APB), the thesis would be graded with 5,0 and counted as one failed examination attempt. The thesis may only be repeated once. In the submitted thesis the written copies and the electronic version for archiving are pursuant to §23 paragraph 7 of APB identical in content.

Darmstadt, August 29, 2023

Saumya Jha

Abstract

The evolution of technology has led to an increasing demand for data in both customer- and industry-specific applications. The current infrastructure is capable of meeting the present requirements. However, as data-centric applications continue to advance, recent statistics on consumer behavior indicate an exponential growth in bandwidth requirements. This necessitates the adoption of new technologies that can exploit more efficient methods in addition to the existing architecture. Optical communications currently heavily rely on single-mode fibers (SMF) with wavelength division multiplexing (WDM), which is efficient but needs to address the issue of "Capacity crunch" in the coming years. One proposed solution involves exploring other dimensions with optimized algorithms to achieve higher data rates. A particularly promising multiplexing scheme that has been extensively researched in recent years is space division multiplexing (SDM), which involves transmitting data through multiple spatial paths in the space domain. This can be achieved using multimode fibers (MMF), multi-core fibers (MCFs), or a combination of these techniques, such as few mode fibers (FMF), which utilize a single fiber with a sufficiently large core to carry multiple modes. Upgrading the transmitter, receiver, and various processing schemes allows for spatial filtering, resulting in increased capacity and reduced cost per bit. To reconstruct the transmitted signal and mitigate challenges or impairments in the network, digital signal processing (DSP) offers a variety of algorithms with pre- and post-processing techniques. One interesting approach is to blindly reconstruct the signal from the transmitted signal without knowledge of the training sequence, using popular blind algorithms adaptively. In this thesis work, we study and discuss the constant modulus algorithm (CMA), multi-modulus algorithm (MMA), and decision-directed feed-forward equalization (DDFFE) for PS QPSK (polarization-switched QPSK) and PDM 16 QAM (polarization-division multiplexed 16 QAM). The proof of concept for few-mode fibers in the back-to-back case is validated through simulations and an experimental setup. The primary focus of this work is on linear effects such as chromatic dispersion, polarization modal loss, additional noise, and crosstalk. The performance of the adaptive blind equalization schemes is measured using the bit error rate (BER) and error vector magnitude (EVM) metrics for all modes with X and Y polarization.

Contents

1 Introduction

Technical innovation and industrial advancement have greatly contributed to the rapid growth of digitization and the availability of high-speed communication systems. The deployment of 5^{th} Generation (5G) communications, along with the extended support of IoT 4.0 standards, has paved the way for a new era of integrated smart solutions that incorporate artificial intelligence and machine learning. These advancements have significantly transformed consumer behavior and technological reliance.

According to estimates in the Ericsson Mobility Report, the total mobile network traffic is projected to reach 472 Exabytes by the end of 2028, accounting for 80% of data traffic[1].

1.1 Motivation

In the field of optical communications, the demand for data is expected to increase by more than 1.5Pbit/s by 2030[2]. This poses a challenge in terms of capacity limitations for bandwidth-intensive applications. To overcome the scarcity of available frequencies, new technologies have emerged that explore new dimensions for data transmission.

Experimental results in the field of space division multiplexing (SDM) have shown the potential to achieve data rates exceeding 10 Pbit/s over multicore fibers. This achievement has been made possible through the use of SDM-optimized fibers, enhanced channel reception schemes, and digital signal processing techniques at the receiver[2].

Researchers are currently analyzing and evaluating methods for the real-time implementation and development of a real-time SDM demonstrator [2]. As these advancements have led to an increase in factors such as noise, crosstalk, and dispersion, the quality of signal reception has been affected. To compensate these effects, digital signal processing schemes play a crucial role at the receiver end [3].

Over the past 40 years, the average capacity of optical networks has experienced a yearly growth rate of 40%, thanks to network evolution and standardization efforts [4]. This consistent increase in capacity has been challenging in meeting the growing demands for data transmission.

In the last decade, data consumption has continued to grow rapidly, driven by bandwidth-intensive services such as video streaming, cloud computing, and machine-to-machine communications. These services alone account for approximately 80% of the total internet traffic [4].

Figure 1.1 illustrates the progression of system capacity over fiber systems, showcasing advancements made with already implemented, or possibly available solutions over several years as it approaches the Shannon limit. To address this, various methods can be implemented, such as reducing power between optical interfaces or incorporating additional

elements to amplify signal power [5]. However, the main driving factor for successful deployment of these additional elements in the future is the goal of achieving reduced cost per bit, energy-efficient systems, and improved spectrum utilization.

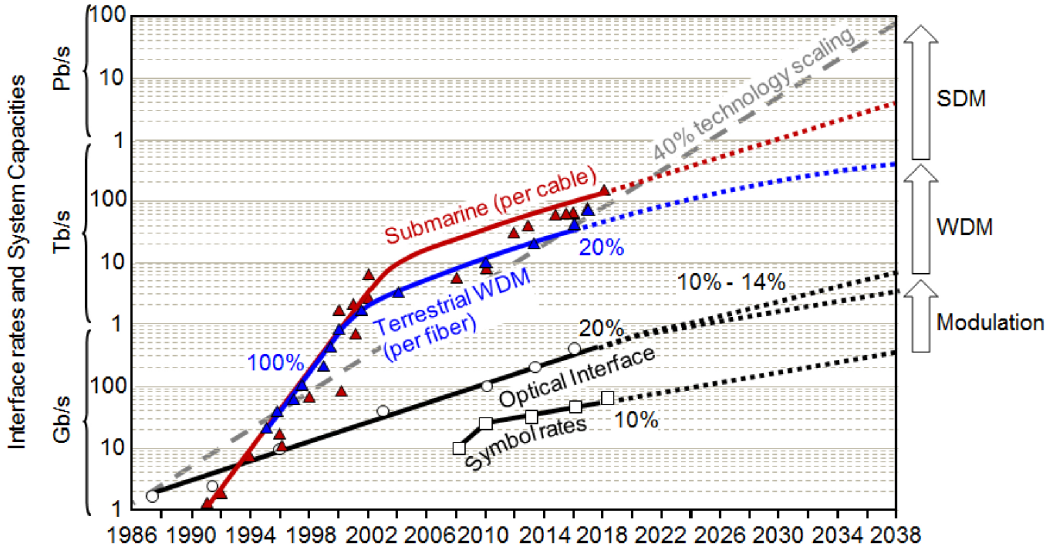

Figure 1.1: System Capacity Comparison for Various Modulation Formats Reprinted from ref. [6]

Note: Figure reprinted from ref. [6], with cross-reference to refs. [7, 8], under a Creative Commons license on 23.08.2023.

1.1.1 Improved Capacity and Spectral Efficiency

To address the capacity demand, one of the fundamental concepts in information theory is Shannon's formula. This formula provides the theoretical upper limit of achievable information rate for a given communication channel and is given by

$$C = B \log_2(1 + SNR) \tag{1.1}$$

This derives the spectral efficiency, $SE = \frac{C}{B}$, and the signal-to-noise ratio as $SNR = \frac{P}{N}$.

It is well-known that a single channel cannot achieve higher capacity, as indicated by the maximum limit derived from Shannon's formula. To double the capacity of a single channel, squared power (or, overall exponential increase by reducing noise) is required. In contrast, when multiple paths are added to this single channel, the required power increases additively. This phenomenon can be attributed to the interplay between the signal-to-noise ratio (SNR) and spectral efficiency (SE), and the impact of multiple modes on gain evaluation[9].

For the sake of simplicity, we can consider SE and C synonymous for a unit bandwidth channel (assuming $B = 1$) in the analysis of gain for a single channel. In the case of a multi-channel system, which may involve different spatial paths with spatial modes or polarization modes, similar considerations can be made.

Firstly, while considering the Gain to achieve fixed SE[9]

$$G_{SE} = \frac{SE^{(M)}}{SE} \tag{1.2}$$

Here, mode M is the product of spatial modes and the number of polarization modes. In the above equation, while assuming the noise in the case of the multi-path channel is identical to the noise of the reference single channel (i.e., $N_m = N$, in all regimes). Similarly, power distribution in each channel is identical (i.e., $P_c = P_m$, for M channels with the same SNR_m, also total SE_m of M channels is M times SE of each channel). Using this formula, we can say that the ratio depends on the number of modes, the corresponding power per channel compared to the power of a single mode channel, and the SNR (Signal-to-Noise Ratio) of the reference channel. The low SNR regime is of particular interest as it demonstrates the maximum impact of reduced power per channel.

Additionally, we can define the SNR per bit for M modes and the gain in energy per bit in terms of spectral efficiency as follows[9]

$$G_E = \frac{SNR_b}{SNR_b^{(M)}} = \frac{2^{SE} - 1}{M[2^{SE/M} - 1]} \tag{1.3}$$

$$\text{where,} \quad SNR_b = \frac{SNR}{SE} = \frac{2^{SE} - 1}{SE} \quad , \quad SNR_b^{(M)} = \frac{2^{SE/M} - 1}{SE/M} \tag{1.4}$$

Equations 1.3 and 1.4 provide the results that indicate that a certain number of M is enough to achieve a significant portion of G_E. However, going beyond 16 does not show much improvement, as reported in the study by [9]. Furthermore, an equal split of signal power brings notable power savings in the case of multiple channels.

The objective here is to increase the overall capacity and optimize the transmission cost per bit in the future. This mathematical expression can be visualized through Figure 1.2, which presents comparative plots of these results.

Therefore, we observe a spectral-efficient multipath multiplexing scheme that utilizes the spatial domain for parallel data transmission in fiber, thereby enhancing the overall capacity offered by Space Division Multiplexing (SDM). In a recent work 1.53Pb/s data rate and spectral efficiency of 332bit/s/Hz was reported to validate this[10]. This technique, known as MIMO (Multiple-Input Multiple-Output) in wireless communications, is currently regarded as the most effective solution in optical communications, offering advantages over traditional Wavelength Division Multiplexing (WDM) techniques.

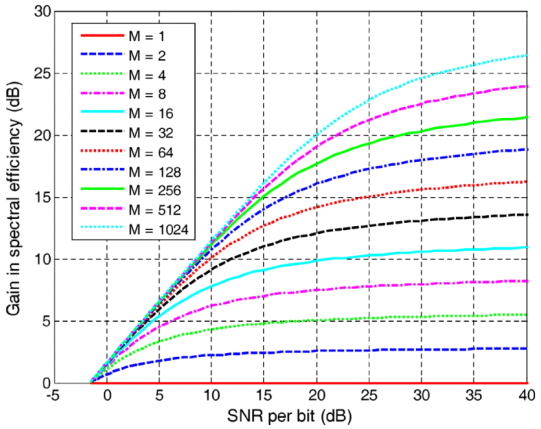

(a) Relation between G_{SE} and SNR per bit of single channel (Equally split single channel power between M independent channels)

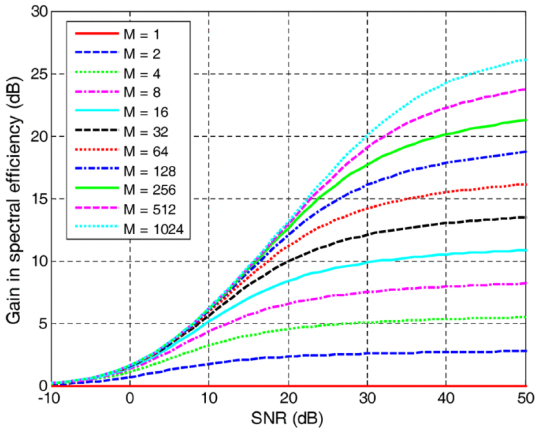

(b) Relation between G_{SE} and SNR

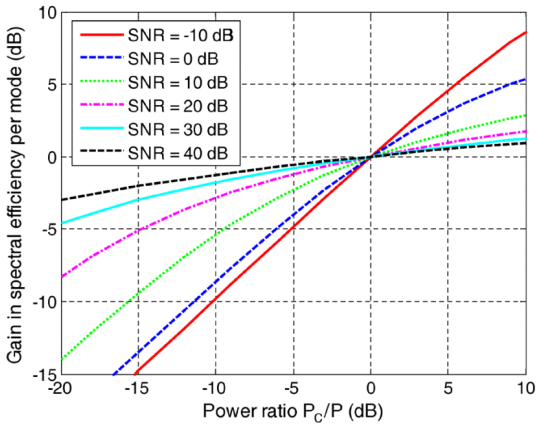

(c) Relation between G_{SE}/M and P_C/P (Power ratio of signal power per mode with power of single channel, independent of number of modes)

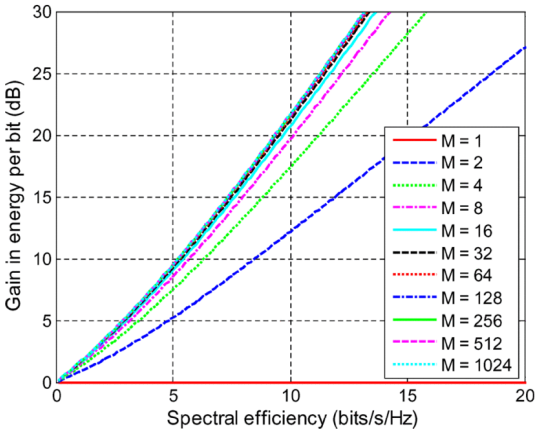

(d) Relation between G_E by using M channels with single channel at same SE with equal power split between all channels

Figure 1.2: Analysis of Improved Spectral Efficiency and Gain for Single Mode vs. Multi Modes [9]

1.1.2 Space Division Multiplexing in Fiber Communication

An advancement over single-mode fiber includes few-mode fibers (FMF), multimode fibers (MMF), and multicore fibers (MCF), which have the potential to enable multiple parallel data transmission through multiple paths within the fiber. Fibers that support multiple spatial modes are referred to as multimode fibers. When the diameter of a single-core fiber is large enough to accommodate multiple modes, it is known as a few-mode fiber (FMF), which can support tens of modes within a single core[11].

Multi-core fibers and space-division multiplexing enable increased capacity by utilizing multiple parallel data streams as separate pipelines with minimal overlap within the same optical fiber[9]. This increases the degree of freedom in the spatial domain. The level of overlap can be adjusted to increase the density of spatial modes by utilizing spatial filtering for multiplexing and demultiplexing purposes[9].

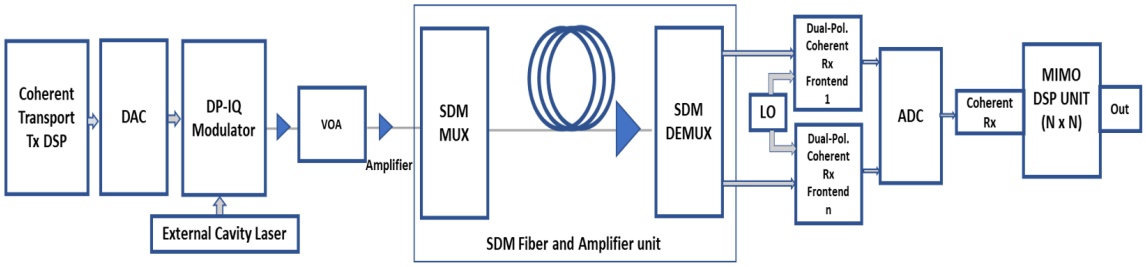

Figure 1.3: SDM System with Transmitter, Channel, and Receiver Unit

Figure 1.3 illustrates the basic SDM (Space Division Multiplexing) optical communication system, which can be divided into three main parts:

- Transmitter: The transmitter employs a DSP (Digital Signal Processing) unit, enhancing overall performance when deployed at both the transmitting and receiving ends. The DAC performs digital-to-analog conversion of the transmit data, comprising the header and payload. The modulated data, along with the carrier, is fed to all the modes by the local oscillator. Additionally, a polarization beam splitter (PBS) may be used for beam splitting, followed by a polarization beam combiner (PBC). An intermediate variable optical attenuator (VOA) allows for adjustment of the OSNR (Optical Signal-to-Noise Ratio) to the desired level. Amplifiers boost the signal, and the transmission occurs over degenerated LP (Linearly Polarized) modes[12].
- Channel: The channel section consists of a multiplexer (MUX) and a demultiplexer (DEMUX) responsible for spatial multiplexing and demultiplexing, respectively. These components propagate the signals through the fiber unit, along with an amplifier such as EDFA (Erbium-Doped Fiber Amplifier).
- Receiver: The receiver section receives the signal at the front end and mixes it with a local oscillator to generate a baseband signal. Subsequently, the electrical in-phase and quadrature components undergo analog-to-digital conversion. The resampled signal is then passed through a coherent receiver and further processed using a DSP unit.

The spatial filtering technique allows for the manipulation of the spatial properties of light, such as intensity, phase, and polarization. These properties can be utilized to control the propagation of data streams through modes, enabling independent transmission[13].

Several components are involved in this technique:

- Mode-selective couplers: These couplers facilitate the coupling of light from one mode to another, enabling mode multiplexing or demultiplexing[14].
- Spatial mode multiplexers and demultiplexers: These components are responsible for combining and separating different modes during transmission.
- Mode converters: These are utilized to change the modes of the transmitted light[15].

In the case of uncoupled multicore fibers, crosstalk is not a significant problem. However, mode coupling between modes or cores can occur, resulting from interference between the various modes or cores within the fiber. This coupling can lead to certain challenges:

- Dispersion: Modal dispersion arises due to different propagation velocities, resulting in inter-symbol interference (ISI) that deteriorates signal quality[16].

- Coupling: Coupling causes unwanted interaction between different modes, degrading overall capacity and performance[17, 16].

Additionally, mode-dependent loss (MDL) refers to the reduction in signal strength caused by power transfer between various modes due to coupling[18].

Optical fibers can have various modes and cores, which contribute to the spatial channels within a fiber bundle, such as a bundle of single-mode fibers (SMFs). Single-mode fiber can be used independently or in combination with few-mode fibers and multicore fibers to enhance capacity. Fiber design and mode multiplexing techniques can be employed to mitigate crosstalk and other impairments[16].

However, it is important to note that higher modes can introduce challenges such as increased crosstalk and dispersive effects. These issues tend to worsen beyond a certain point as more modes are utilized.

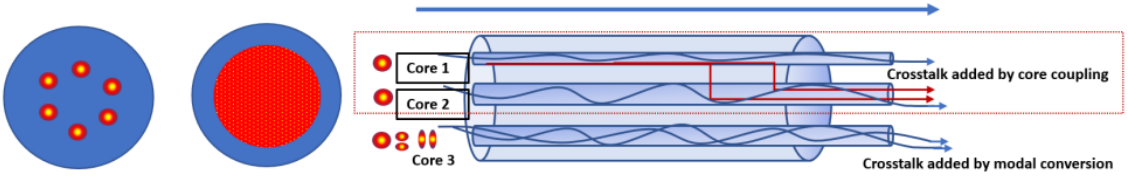

Figure 1.4: (a) Multi-Core Fiber (MCF) and Multi-Mode Fiber (MMF) (b) Crosstalk Demonstration in Multi-Core Fiber (MCF) and Multi-Mode Fiber (MMF) within the Same Fiber[17]

As the number of modes and cores increases in multimode fibers or multicore fibers, the likelihood of higher crosstalk, mode coupling, and modal dispersion also increases. These impairments not only limit the system performance but also restrict the achievable data rate. They can be caused by fiber imperfections or perturbations that occur during transmission. However, these effects can be mitigated to a certain extent through the use of spatial filtering techniques and efficient DSP with robust algorithms.

The DSP unit plays a crucial role in reconstructing the transmitted signal to ensure better signal quality while maintaining energy efficiency[19]. In optical communications, linear and non-linear effects can degrade the quality of received signals. Non-linear effects such as the Kerr effect, self-phase modulation, and cross-phase modulation distort the received signal. Linear amplitude stimulated emission can also contribute to noise. Additionally, intrinsic material properties and dispersion can cause signal degradation. Various non-linear techniques have been proposed to address these challenges. It is essential to synchronize the transmit and receive signals in terms of phase and frequency.

In this work, the focus is primarily on linear effects such as chromatic dispersion (CD) and polarization modal dispersion (PMD) in single-mode fibers (SMFs), as well as modal dispersion and crosstalk in multimode fibers (MMFs) or multicore fibers (MCFs) [20]. The analysis presented here explores adaptive equalization techniques for higher-order MIMO (N x N MIMO) structures in SDM (Space Division Multiplexing) optical communication systems, where the number of transmitters and receivers is equal for a single MMF or MCF.

The digital signal processing unit, in conjunction with optical coherent detection, effectively compensates for linear effects. However, the challenge of reducing energy consumption while achieving higher capacity remains a major concern for the next generation of communications [3]. As infrastructure advances, algorithm complexity and processing requirements become

more power-intensive. Therefore, it is worth revisiting classic algorithms and lower-order modulation schemes for signal acquisition at the receiver.

Traditionally, known training sequences have been widely used at the receiver. However, these may not be the preferred choice when bandwidth constraints exist. The reason is that pilot sequences need to be decoded at the receiver and are sent as part of the sequence header, occupying a portion of the bandwidth. In scenarios where bandwidth constraints are a concern, approaches that eliminate the need for additional training sequences become more attractive[21].

These equalization techniques are commonly referred to as blind equalization techniques. They rely solely on signal statistics, such as signal amplitude or knowledge of the constellation, to infer the transmitted constellation during the acquisition stage. This is followed by the tracking and recording stage. Numerous algorithms exist that can perform these tasks effectively.

1.2 Task Description

As previously mentioned, the digital signal processing unit at the receiver plays a crucial role in compensating for degradation and reducing impairments. It equalizes the distortions and aims to recover the transmitted signal. In this thesis, we focus on linear impairments, specifically those caused by chromatic dispersion, polarization losses, inter-mode crosstalk, inter-core crosstalk, and mode-dependent losses (MDL). To address these impairments, we primarily consider linear equalizers. The main objective of the thesis are as follows

1. Study the implementation of MIMO equalizers in Space Division Multiplexing (SDM) systems.
2. Implementation of a MIMO equalizer into an offline data processor into Matlab.
3. Validate the implementation of the MIMO equalizer by numerical simulations and potentially with lab measurements.

In this thesis, the main focus is on classic equalization algorithms, particularly the Constant Modulus Algorithm (CMA), Multi Modulus Algorithm (MMA), and the non-linear Decision-Directed Least Mean Square Algorithm (DDLMS). These algorithms are employed after achieving pre-convergence using any of the aforementioned linear equalizers.

1.3 Outline

This thesis is organized into six chapters, followed by the bibliography and appendix sections. Chapter one serves as the Introduction, providing a comprehensive overview of the work and outlining the structure of the thesis. Chapter two focuses on the state-of-the-art algorithms, highlighting relevant information and discussing ongoing novel approaches for various scenarios. Chapter three presents the mathematical representation and objective function of the equalizer, which are essential for the implementation of adaptive blind equalization algorithms. The discussion is extended in chapter four, where the chosen conditions and experimental setup used for evaluating the task are described. The main highlight of the work is covered in chapter five, which includes the analysis and presentation of the obtained results. Finally, chapter six concludes the thesis by offering final remarks related to the task and discussing potential areas for further research and exploration in the future.

2 Fundamentals of Digital Signal Processing in Optical Communications

Communication over optical networks can be significantly affected by various distortions caused by material properties, dispersion, and coupling between different modes. Non-linear impairments can be mitigated partially using backpropagation and other non-linear filtering techniques [22]. Chromatic dispersion (CD) and polarization mode dispersion (PMD) are major contributors to linear impairments in fiber transmission.

These linear impairments can be effectively compensated by using digital coherent receivers, which are capable of mitigating phase and polarization distortions and mapping the optical field into the electrical domain [20]. In addition to that, other multi-mode/core effects in the fiber, linear equalization techniques are sufficient[17].

In this work, we specifically focus on the linear degradations caused by CD, PMD, and other multi-mode/core effects in the fiber. Linear equalization techniques prove to be effective in compensating for these combined effects[19]. Chromatic dispersion occurs because waves with different wavelengths travel at different speeds depending on the refractive index of the fiber material[19]. This leads to a delay and broadening of the optical pulse over time, ultimately limiting the overall data rate.

PMD, on the other hand, is caused by birefringence, where different orthogonal polarization modes experience different delays[23]. This results in the spreading of the optical pulse, causing inter-symbol interference and degrading signal quality. PMD also limits the overall capacity of the system. The birefringence can be caused by asymmetry or external factors, which can be mitigated up to an extent through optimized fiber design.

The integration of a digital signal processing (DSP) unit with the coherent receiver further enhances the effectiveness of compensation, providing a lower complexity solution compared to optical homodyne detectors. After digitizing the received signal, tracking is performed to compensate for phase and frequency offsets resulting from the mismatch between the local oscillator and the incoming signal. Forward Error Correction (FEC) is then applied to improve the overall system performance [20].

Coherent receivers can rely on either blind adaptation methods or training sequences, depending on the availability of signal information and specific requirements. Equalization can be performed in two stages, initially compensating for chromatic dispersion, which is a polarization-independent effect, followed by compensation for polarization mode dispersion (PMD). This approach allows for adaptation to different rates and properties of these effects [17, 20].

2.1 Coherent Receivers with Digital Signal Processing

As mentioned earlier, coherent detection combined with digital signal processing is highly beneficial in mitigating linear impairments. In this section, we introduce the DSP modules at the receiver, as depicted in Figure 2.1. This differs from data-aided equalization and includes blind equalization subsystems.

In the simulation setup, it is not necessarily required to have chromatic dispersion (CD) compensation. Instead, we focus on pre-and post-frequency offset recovery units along with equalizer stage 1.

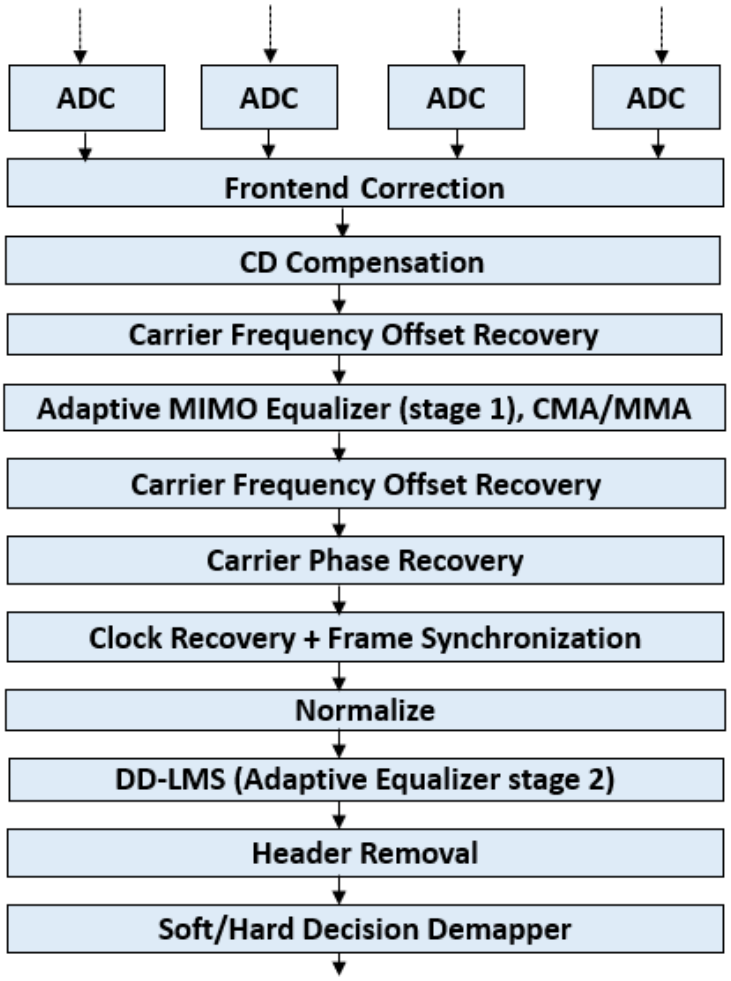

Figure 2.1: Coherent Receiver and DSP Subsystems

Figure 2.1 depicts the coherent receiver combined with a DSP unit. While Chapter 1 explains some of the basic subsystems, there are additional modules introduced:

- Carrier frequency estimation corrects the frequency offset. The receiver incorporates carrier frequency offset recovery in two stages, one before the blind equalization stage and an additional unit after the first stage of equalization.
- Normalization ensures the correct amplitude of the received signal.

- Two-stage digital equalization compensates for impairments introduced during channel propagation. The first stage compensates for channel-induced crosstalk, while the second stage compensates for frontend-induced impairments.
- Clock recovery determines and corrects timing errors in the received signal.
- Interpolation rectifies timing errors by interpolating the received signal.
- Carrier phase estimation mitigates phase errors of the carrier signal[19].
- Deskew performs temporal alignment of the digital signal.

These additional modules, working in conjunction with the coherent receiver and DSP unit, enhance performance and compensate for impairments introduced during channel propagation.

The fiber channel can be regarded as a concatenation of filter elements with the inclusion of a noise source. In optical communication systems, the primary source of noise is typically the Erbium Doped Fiber Amplifier (EDFA) which introduces Amplified Spontaneous Emission (ASE) noise. To estimate the transmitted signal, the receiver takes into account the band-limited channel, along with the presence of Additive White Gaussian Noise (AWGN) and other performance-limiting factors such as crosstalk.

In many cases, the receiver is provided with a training sequence in the form of a fixed-length preamble block. This training sequence plays a crucial role in the estimation and recovery process. Equalization, in this scenario, necessitates knowledge of the channel impulse response, and the inversion of the channel matrix is performed to obtain an estimate of the transmitted data[3].

When utilizing a training sequence, the auto-correlation and cross-correlation properties are often exploited. Alternatively, shift-orthogonal sequences created through cyclic shifting can be employed. A widely used option for complex training sequences are the Constant-Amplitude Zero Auto-correlation (CAZAC) sequences, which offer ideal cyclic auto-correlation properties regardless of the length of the training sequence[3]. Additionally, pre-compensation techniques can be employed to mitigate the effects of the scalar Chromatic Dispersion (CD) in an uncompensated link. This approach serves to reduce the length of the Multiple-Input Multiple-Output (MIMO) equalizer and the required training sequences.

Overall, considering these aspects ensures efficient estimation and recovery of the transmitted data in the presence of noise and other performance-limiting effects in optical communication systems.

2.1.1 MIMO Equalization

MIMO equalization can be performed either in the time domain or in the frequency domain using distance-minimizing algorithms.

In the case of frequency domain equalization (FDE), the overall complexity is lower when using long filters[18, 24, 25]. However, for shorter distances, time domain equalization (TDE) has lower complexity.

In general, implementing FDE offers reduced complexity and a bandwidth-efficient scheme, making it widely used[24, 18, 21]. This approach, also known as data-aided equalization, provides stable performance independently of the modulation format in the payload, allowing

for scalable receiver design. Figure 2.2 illustrates an example of FDE using overlap-save processing for a 2×2 MIMO system. The overlap factor can be adjusted as needed[26].

The filter adaptation function is responsible for computing the tap values of the equalization matrix coefficients, aiming to estimate the output as closely as possible to the input. The objective function in this case seeks to minimize the mean square error (MSE) to reduce overall distortion, assuming a joint wide sense stationary stochastic process with zero mean for the input and desired output. By setting the derivative of the cost function to zero, the optimal value can be obtained. Minimizing the MSE leads to the Minimum Mean Square Error (MMSE) equalizer, which can be computed using the Least Mean Square (LMS) algorithm with low complexity for the update function[27, 3].

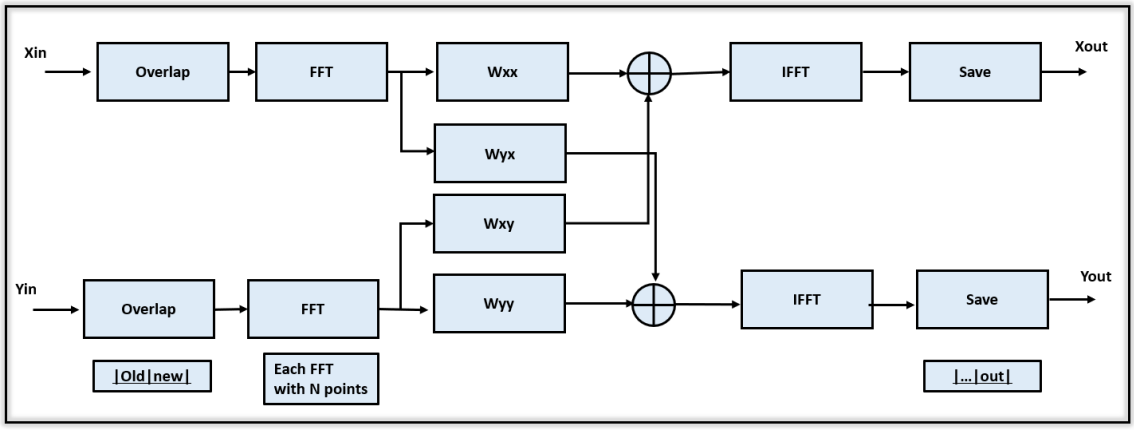

Figure 2.2: Frequency Domain Filtering with Overlap-Save Processing and Overlap Factor for 2×2 MIMO

Blind equalization algorithms, or blind source separation (BSS), provide attractive alternatives to training-based approaches. In blind equalization, the equalization is performed without any prior knowledge of the input signal or channel values. It relies solely on the properties or statistics of the received signal. This leads to faster acquisition and reduced overall overhead, as there is no need for a preamble block or training sequence in the header, resulting in reduced packet overhead and more efficient bandwidth utilization. Therefore, this approach is preferred when efficient bandwidth utilization with reduced overhead is a primary concern. It assumes independent and identically distributed (i.i.d.) symbols[27].

As mentioned earlier, blind equalization can be performed in both the time and frequency domains. Finite impulse response (FIR) filters or infinite impulse response (IIR) filters can be used, but FIR filters are preferred due to their stability, linear phase response, and ease of implementation[28].

Mathematically, this can be explained by modeling the dispersion compensating filter (DCF) in the time domain, which provides an upper bound on the number of filter taps. While converging to the Wiener filter solution is considered ideal, utilizing the physics or prior knowledge of the underlying system can provide an intuitive closed-form solution to the problem.

By using the derivative form of the pulse envelope and transforming it into the frequency domain, we obtain the transfer function. Taking the inverse of the transfer function and convolving it with the arbitrary input signal gives us the impulse response of the CD compensating filter[20]

$$g_c(z,t) = \sqrt{\frac{jc}{D\lambda^2 z}} \exp(-j\phi(t)) \quad \text{where,} \quad \phi(t) = \frac{\pi c}{D\lambda^2 z} t^2 \tag{2.1}$$

Where, D represents the dispersion coefficient of the fiber, z represents the propagation distance with time variable t within a frame, λ represents the wavelength, and c represents the speed of light.

Implementing the filter in the digital domain poses several challenges. The equation is non-causal and has infinite duration, leading to aliasing due to finite sampling frequency and passing of all frequencies. Consequently, a very high number of filter taps is required. To address this, the impulse response (IR) of the filter is truncated using windowing techniques, allowing for the realization of the filter digitally with a sufficient number of taps. The obtained tap weights are then used for chromatic dispersion (CD) compensation. A static filter can be used to compensate for most of the CD, while an adaptive equalizer can handle residual dispersion.

The upper bound for the number of taps in a specific frequency range is determined by $\frac{-0.5}{T} \leq f \leq \frac{0.5}{T}$. By adjusting the number of taps for a particular frequency f, a constant dispersion can be achieved within this frequency range. Additionally, to model the polarization-dependent effects on wave propagation, a non-unitary Jones matrix can be utilized. Estimating and inverting this matrix adaptively helps mitigate impairments[20].

The equalizer's task is to compute the filter coefficients and update them with each iteration based on the received signal. The objective is to minimize the cost function by taking the gradient and setting it to zero. This allows convergence towards the optimum solution, which can be achieved using techniques such as stochastic gradient descent or ascent.

In the context of blind equalization with stochastic gradient descent (SGD), the problem of multiple local minima can lead to singularities and convergence issues. Choosing the appropriate step size is crucial as it affects the algorithm's performance. Both too-large and too-small step sizes can hinder convergence[19].

The suitable range of step sizes can vary depending on factors such as the number of input symbols, added crosstalk and noise, window length, and other parameters. This is discussed and demonstrated in Chapter 4, which presents the error curve. For adaptive blind equalization in the time domain, the least mean square (LMS) method is commonly used, along with some derived approaches.

In the context of multimode or multicore fiber systems, the equalizer implemented with a coherent optical receiver should be capable of tracking the time-varying polarization state after the acquisition step. This time-varying effect is caused by the birefringence of the fiber material[29].

However, in the case of links with potentially high levels of modal dispersion, implementing MIMO equalizers with a large number of taps becomes challenging. Addressing this issue is crucial for achieving effective equalization in such systems.

2.2 State of the Art

In recent years, researchers have proposed novel algorithms, including those based on machine learning, to compensate for non-linear effects in equalization. These algorithms

often build upon state-of-the-art techniques such as recursive least squares (RLS) or the constant modulus algorithm (CMA)[18].

RLS is an efficient algorithm that minimizes the mean square error (MSE) recursively. However, its complexity increases as a drawback[16].

CMA is particularly attractive for scenarios with bandwidth constraints and faster acquisition. It exploits the property of constant amplitude and works well with low-order modulation schemes like BPSK and QPSK. Research has demonstrated that PDM (Polarization division multiplexed) QPSK (Quadrature Phase Shift Keying) improves overall efficiency by doubling the transmission rate compared to DP (Dual Polarization) QPSK. Therefore, PDM QPSK has been widely adopted in classic algorithms [19].

CMA requires an additional carrier phase recovery unit and can only equalize based on the received signal amplitude. While CMA is robust in the presence of noise, it may amplify noise signals when the received signal is highly correlated with noise. Therefore, CMA is not suitable for signal tracking, and alternative algorithms or extensions to CMA are needed for better acquisition and tracking performance [3].

CMA can also be used with lower-order QAM and still yield good results, even though the constant modulus property is violated. However, in such cases, a larger number of input symbols is typically required.

As an extension to CMA, multi-modulus algorithms (MMA) can be employed in cases where the constant modulus property is not applicable. MMA does not impose a condition of fixed average power in the error calculation. Instead, it utilizes different rings with varying power levels, resulting in enhanced performance. MMA can be used for both acquisition and tracking and tends to provide good results for higher-order modulation schemes[3].

Decision-directed equalization (DDE) is a popular non-linear approach that uses decision-based criteria to recover the constellation in a second step, following the pre-convergence achieved using algorithms like CMA or MMA. DDE focuses on the reference and received points rather than the power level of the constellation, allowing it to compensate for phase offsets and produce a high-quality received signal constellation. However, DDE typically requires pre-conditioning of the filter coefficients to ensure good convergence, as it may have poor convergence in the absence of such pre-conditioning[29].

On the other hand, least mean square (LMS) algorithms work well with known training sequences and ensure convergence towards the global minimum, regardless of the initialization conditions. This is in contrast to CMA, where the complete blindness of the algorithm can lead to multiple local minima, often influenced by the initialization of tap weights. Therefore, LMS can be used as a second step in equalization, in combination with a decision-directed feedback system[30].

Another non-linear approach is the Maximum Likelihood Sequence Estimator (MLSE), which utilizes statistical properties and the statistical model of the transmitted sequence to estimate the sequence accurately.

2.3 Related Work

In the realm of MIMO digital signal processing (DSP) for spatial division multiplexing (SDM), various approaches have been proposed to optimize performance and energy consumption.

Recent advancements have seen the combination of novel algorithms with classic blind equalization techniques in optical and wireless communication systems.

Previous demonstrations have shown that 16-QAM is a favorable choice for achieving high-speed data rates using state-of-the-art DSP algorithms such as CMA and MMA, combined with coherent detection. This combination proves to be effective in mitigating chromatic dispersion (CD), polarization mode dispersion (PMD), and crosstalk, thereby improving performance in MIMO structures[31].

For higher-order QAM, assuming a fractionally spaced equalizer, extensions of MMA have been proposed, including the multimodulus radius-directed algorithm and the symbol-based decision algorithm. Additionally, the regional multimodulus algorithm addresses challenges related to convergence speed and divergence by incorporating adjustment with initialization parameters. These algorithms aim to converge towards the Wiener filter solution to minimize misadjustment in steady state[32, 33, 34].

Independent component analysis (ICA) is another blind source separation technique used in MIMO DSP. It assumes uncorrelated source signals with non-Gaussian distributions and makes use of the central limit theorem to maximize the relative distance from the Gaussian distribution of individual components. ICA applies a pre-whitening matrix, followed by principal component analysis using singular value decomposition until the projection yields maximum variance[35].

A model-based approach was proposed for optical communications utilizing linear butterfly finite impulse response (FIR) filters in conjunction with a variational autoencoder equalizer. The goal was to address convergence issues associated with classic CMA by employing variational inference to approximate the maximum likelihood criterion for higher-order probabilistic constellation shaping (PCS). This approach also allows for potential extensions with various machine learning techniques, enabling joint communication and sensing capabilities[36, 37].

In the context of terahertz band wireless communication systems, a neural network-based Joint Deep Belief Network (J-DBN) approach was proposed alongside CMA and DD-LMS. The aim was to integrate fiber-wireless communication for lower cost, reduced power consumption, and increased capacity, with an offline experimental demonstration conducted for a 2x2 MIMO link using QPSK over standard single-mode fiber (SSMF). The results showed a reduction in computation complexity, improved computational time, better training accuracy, enhanced signal-to-noise ratio (SNR) gains, and improved bit error rate (BER) for receiver sensitivity[38]. However, it is worth noting that the specific interest lies in multi-mode fiber (MMF), few-mode fiber (FMF), and multi-core fiber (MCF) systems.

3 Problem Formulation

The linear distortion experienced by the received signal as it traverses an unknown channel during transmission can be mitigated through the utilization of either a known training sequence or statistical properties of the signal. In Chapter 2, the mathematical representation for compensating for impairments such as chromatic dispersion (CD) and polarization mode dispersion (PMD) was thoroughly discussed, highlighting the significance of equalization techniques and pertinent filter parameters.

The primary objective is to estimate the channel effects at the receiver and effectively reverse the distortions encountered during the recovery process of the received signal. This is accomplished by employing well-established equalization methods and algorithms that adapt the coefficients of the equalizer based on characteristics observed in the received signal. The ultimate goal is to minimize the discrepancy between the expected signal and the received signal, thereby effectively mitigating the adverse effects of channel distortion.

Problem Formulation: When a transmitted training sequence is not available at the receiver, estimation can be done using Blind algorithms. These algorithms rely on the statistical properties or signal characteristics of the received signal to estimate the channel effects without prior knowledge of the transmitted training sequence[20].

Blind Equalization: Estimate the transmitted signal at the receiver by utilizing the signal statistics, such as the shape or power of the received signal. The input to the blind equalization algorithm is the received signal, denoted as a discrete-time sequence of complex-valued samples $y[n]$, where n represents the sample index. The channel coefficients h_{ij} and equalizer coefficients w_{ij} are utilized in the numerical analysis for blind equalization[20].
Approach: The Task of the filter adaptation function in blind equalization is to compute the tap values of the equalizer coefficients (W) to generate an output signal that closely matches the true transmitted signal. This is achieved by minimizing the error(ϵ) between the expected signal and the received signal. The choice of the cost function depends on the specific requirements of the application. Some commonly used cost functions in blind equalization include

1. Mean Square Error(MSE): The cost function is defined as the average square difference between the expected signal and the received signal. The goal is to find the optimal coefficients that minimize the expectation of the difference between the desired and equalized signals[18].

2. Maximum Likelihood Estimation: The cost function is defined as the logarithm of the likelihood function. This estimation is based on the statistical distribution of the received signal, such as a Gaussian distribution. The objective is to find the optimal equalizer coefficients that maximize the probability of observing the received signal[36].

3. Constant Modulus: This cost function is suitable for transmitted signals with a constant modulus property, where the amplitude is known but the phase is not. The cost

function aims to minimize the deviation from the constant modulus constraint, making it well-suited for low-order modulation schemes with robust performance. However, the performance may degrade when the constant modulus property is violated or when the noise signal dominates over the desired signal.

The objective function is given by

$$W_{opt} = \arg\min_{w}(\epsilon) \tag{3.1}$$

In blind equalization, the update of equalizer taps can be performed using various algorithms such as the Constant Modulus Algorithm (CMA), Recursive Least Squares (RLS), or Least Mean Squares (LMS), as discussed in Chapter 2. The objective is to converge toward the optimum solution by minimizing the chosen cost function over a certain number of iterations.

To update the equalizer taps, the gradient of the cost function with respect to the filter coefficients is computed. Optimization algorithms like Stochastic Gradient Descent (SGD) can be employed to iteratively update the equalizer taps based on the gradient information. SGD adjusts the filter coefficients in a way that moves towards the minimum of the cost function, thereby improving the equalization performance.

By iteratively updating the equalizer taps using the chosen algorithm and optimizing the cost function, the blind equalization process aims to converge toward the optimal solution, effectively compensating for channel distortions and improving the accuracy of the recovered transmitted signal.

3.1 Channel Model and System Setup

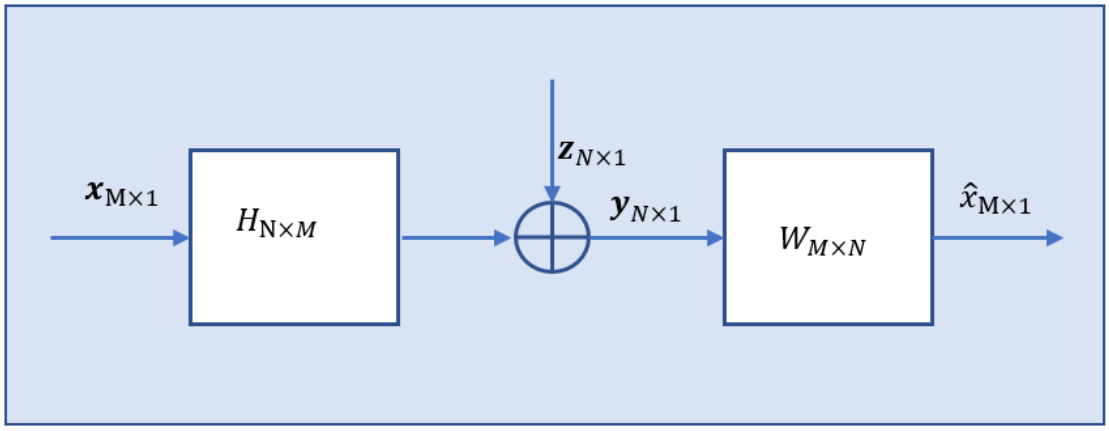

Figure 3.1: Simplified Channel Model with Equalizer

The linear time-invariant channel model for the MIMO System is given as

$$y_{N\times1} = H_{N\times M} \cdot x_{M\times1} + z_{N\times1} \tag{3.2}$$

$$\text{alternatively,} \quad y[n] = \sum_{m=1}^{M} \mathbb{H}[n,m] \cdot x[m] + z[n] \tag{3.3}$$

where elements of vectors $x_{M\times1}$, $y_{N\times1}$, $H_{M\times N}$, $z_{N\times1}$ are vectors of dimensions $x_{M\times1\times xLength}$, $y_{N\times1\times yLength}$, $H_{M\times N\times hLength}$ and $z_{N\times1\times yLength}$ respectively. The above equation can be rewritten in the time domain as the convolution between matrix $H_{M\times N}$ and vector $x_{M\times1}$ for time instant p as

$$y[n](p) = \sum_{m=1}^{M} \left[\sum_{q=0}^{l-1} \mathbb{H}[n,m](q) \cdot x[m](p-q) \right] + z[n](p) \tag{3.4}$$

$$l = min(hLength, xLength)$$

Here n and m are iteration indexes over the N and M elements of the the vectors $y_{N\times1\times yLength}$, $x_{M\times1\times xLength}$ and the channel matrix $H_{M\times N}$. Similarly, p and q iteration indexes are used for each element in the vectors and channel matrix in the discrete-time dimension. Here $xLength, hLength$ denote the length of the transmitted signal vector and the channel matrix in discrete time dimensions respectively.

MIMO equalization matrix: Using equation (3.1), the Time-domain MIMO equalization matrix $W_{M\times N}$ can be defined to obtain an estimation of the system input signal $x_{M\times1}$ as mentioned below

$$\hat{x}_{m\times1} = W_{M\times N} \cdot y_{N\times1} = W_{M\times N} \cdot (H_{N\times M} \cdot x_{M\times1} + z_{N\times1}) \tag{3.5}$$

We perform convolution in the time domain for time instants p and q, similar to the equation (3.3), and shifting $y[n]$ by $wLength$. Here this shift in $y[n]$ does not change the nature of the representation of the equation, as mentioned below

$$\hat{x}[m](p) = \sum_{n=1}^{N} \left[\sum_{q=0}^{wLength-1} \mathbb{W}[m,n](q) \cdot y[n](p-q+wLength-1) \right] \tag{3.6}$$

To evaluate it further, we do the **batch processing** of $y[n]$ by defining a reversed time batch of size $wLength$ with p batches Samples per Symbol (SPS) as

$$\tilde{y}^p[n] = y[n](wLength-1+p*SPS : -1 : p*SPS) \tag{3.7}$$

$$\text{further,} \quad \hat{x}^p[m] = \hat{x}[m](p) = \sum_{n=1}^{N} W[m,n] \cdot \tilde{y}^p[n] \tag{3.8}$$

This batch processing is done in the time domain and gives impressive results.

3.2 Algorithms

The choice of algorithm for blind equalization depends on the specific application requirements. In this context, we will discuss three popular classic blind algorithms that have demonstrated efficiency. Figure (3.2) depicts the contour and decision boundary of these algorithms, which are utilized in simulations and experiments.

It is important to note that without further context or information, the specific algorithms and their associated properties cannot be elaborated upon. However, the figure serves as a visual representation of the algorithms' performance and their ability to accurately separate decision boundaries in a given application scenario.

3.2.1 CMA

CMA utilizes the constant modulus property of the transmitted signal, hence it works well with lower-order modulation schemes. It can be used for the acquisition of 16-QAM as well despite the nonconstant modulus, however the performance degrades with the increase in the order. CMA can be combined with stochastic gradient descent (SGD) to achieve convergence towards the optimum solution[20].

While CMA is robust in the acquisition phase, it may not perform as well in the tracking phase. Therefore, it is often used in conjunction with a second stage of equalization to further compensate for front-end impairments. Additional units can be employed to enhance phase and frequency components.

It is important to note that CMA primarily focuses on the amplitude of the received signal and does not explicitly consider the phase in the acquisition stage. As a result, an additional carrier phase recovery stage is required. The update rule for the equalizer taps in CMA imposes constraints on the constant modulus while minimizing the error using SGD, $|s_k| = 1 \forall k$. Possible solution is to look for coefficient W such that, $|y_k| = 1 \forall k$. The Equalizer tap update rule is given as

$$W^{j+1}[m,n] = W^{j}[m,n] + \mu \epsilon_m^j \hat{x}^j[m](\tilde{y}^j[n])^* \tag{3.9}$$

Error function ϵ_m for the j^{th} iteration is calculated as

$$\epsilon_m^j = (|\tilde{x}^j[m]|^2 - P_{0,m}) \tag{3.10}$$

Here, $P_{0,m}$ is the average power of the reference constellation for the lane/path m. This reference power is fixed based on the type of modulation scheme(lower order with constant modulus property), and the received signal power is compared with it. This allows the algorithm to assess the deviation from the constant modulus property and make appropriate adjustments to the equalizer taps to minimize the error. By comparing the received signal power with the reference power, CMA can effectively equalize the signal while maintaining the desired constant modulus property.

3.2.2 MMA

The Multi Modulus Algorithm (MMA) is an extension of the Constant Modulus Algorithm (CMA) that is used for equalization in communication systems. It addresses the issue of violating the constant modulus property for constellations with higher orders. MMA aims to minimize the mean square error (MSE) by adjusting the equalizer taps based on the distance between the received signal power and different radii or power levels associated with the rings formed by these levels. The tap update rule in MMA is similar to CMA, but the error calculation rule is modified to account for the violation of the constant modulus property and the use of multiple power levels or rings. This modification allows MMA to effectively

equalize constellations with higher orders and improve equalization performance. The tap update rule is given by

$$W^{j+1}[m,n] = W^{j}[m,n] + \mu\epsilon_m^j \hat{x}^j[m](\tilde{y}^j[n])^* \tag{3.11}$$

The error update rule is given by the following equation

$$\epsilon^2 = (|x_{out}|^2 - P_{MMA})^2 \tag{3.12}$$

As we can see the the tap update rule is similar to CMA, but error calculation rule is different here.

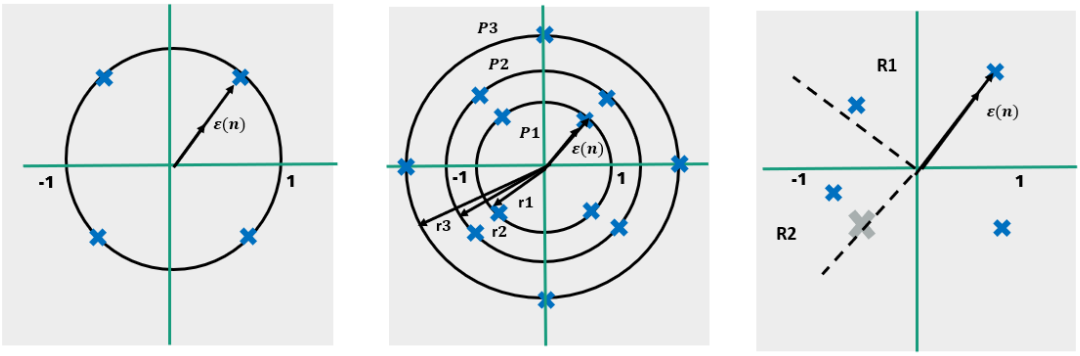

Figure 3.2: (a) CMA Circular Region (b) MMA Rings (c) DD-FFE Decision Boundary

3.2.3 DD-FFE

In decision-directed feed-forward equalization, the least mean square (LMS) algorithm is used to minimize the cost function. This approach is effective when preconvergence has been achieved using algorithms like CMA or MMA. The received constellation is improved by considering a target point in the reference constellation. LMS minimizes the Euclidean distance between the target and received data points, allowing for the enhancement of the constellation by considering both the phase and magnitude of the data points.

The tap update rule in decision-directed feed-forward equalization is slightly different. The processed output signal from the first stage of equalization is treated as the input signal for the tap update process. This allows for further refinement of the equalization process and improvement of the received constellation. The update rule is given by

$$W^{j+1}[m,n] = W^{j}[m,n] - \mu\epsilon_m^j(\tilde{y}^j[n])^* \tag{3.13}$$

Error update rule differs here due to the consideration of reference and received data points instead of the Power values. The error update rule is given by

$$\epsilon^2 = |x_{out} - x_{ref}|^2 \tag{3.14}$$

The result obtained from DD-LMS gives sharp constellation and the phase and frequency offsets are already corrected.

3.2.4 Algorithm Implementation

The algorithm flow remains consistent across all three cases, differing only in the error calculation and filter tap coefficient update functions. For instance, the Constant Modulus Algorithm (CMA) exemplifies this flow. The initialization of the number of taps has been elucidated in Chapter 2. Employing batch processing proves advantageous for augmenting performance in the time domain. Alternatively, time domain equalization can be transformed into the frequency domain by leveraging the Fast Fourier Transform (FFT) and Inverse FFT (IFFT) techniques. In subsequent chapters, we will present experimental results pertaining to the short-length (1 km) Few Mode Fibers (FMF), thereby demonstrating the practical implementation of time domain equalization. Within the CMA algorithm, spatial modes are denoted by row indices, and samples are denoted by column indices. The number of Samples per Symbol (SPS) can be flexibly configured as either 1 or 2, contingent upon specific requirements.

Algorithm 1: Algorithm for CMA

Data: $M, N, W, SPS, P_{0,m}, niterations, IdentityInit, x, \mu, nTaps$
Result: x_{out},$Wopt$,$ErrOpt$,$errInit$
$\epsilon \rightarrow 0$
for $i = 1 : nIteration$ **do**
  Initialization;
  $ErrInit \leftarrow \infty$;
  if $m{=}n$ **then**
    $W^0[m,m](nTaps/2) \leftarrow 1$; / $m = n$ /
  else
    $W^0[m,m] = 0$; / otherwise ($\neq nTaps/2$) /
  end
  Define numberOfBatches for BatchLength 'p'
  $numberOfBatches =$ floor$((yLength/SPS)$
  for $p = 1 : numberOfBatches$ **do**
    Define $batchIdx$
    $batchIdx = batchlength + (p-1) * SPS : -1 : (p-1) * SPS + 1$
    Evaluate $\tilde{x}^{j=0}$ with initialized $W^{j=0}$ and batched received signal $\tilde{y}^{j=0}$
  end
  Save the sample $\tilde{x}^{j=0}$ in x_{out} (the output vector)
  Calculate every $\epsilon_m^{j=0}$
  Update $W^{j=1}[m,n]$
  if $\epsilon < ErrInit$ **then**
    Iterate until $j =$ required number of iteration
    $ErrOpt \leftarrow \epsilon$;
    $Wopt \leftarrow W$;
  end
end

The overall performance of time domain equalization is influenced by several key factors:

- Pre-processing steps are undertaken before stage 1 of equalization.
- Proper initialization of filter coefficients $W^0[m,m]$, as this greatly affects the convergence of the Constant Modulus Algorithm (CMA) and overall performance.
- Selection of an appropriate step size μ, which is crucial for achieving stable and rapid convergence. It may need to be adapted dynamically during the equalization process.
- Careful consideration of tap length (nTap) is necessary to accurately model the channel response, as discussed in Section 2 of the thesis.

These factors collectively contribute to the overall effectiveness and efficiency of the time domain equalization technique.

4 Simulation Setup of Adaptive Equalizers

4.1 Setup and Implementation

4.1.1 Simulation Setup:

A generic code was developed for a $M \times N$ MIMO system, where $M = N$, using batch processing. The simulation and experimental setup includes a two-stage equalization. The focus here remains only on the adaptive blind equalizer for MIMO system stage 1, as depicted in Figure 4.1 of the thesis. For demonstration and experimental simulations, MATLAB with its GUI capabilities was utilized. Although Python or C could have been chosen, we opted for MATLAB due to the availability of existing prototype files in MATLAB.

An existing 2×2 MIMO demo file, served as a reference for evaluating the new demo and experimental setup. The subsequent chapter will provide detailed insights into both the demo and experimental results. In this particular section, our focus is primarily on the MATLAB generic code and offline processing used for validating the theoretical proof of concept.

To initiate the simulation setup, we defined the channel model by specifying parameters such as the number of transmitted modes, number of fibers, modulation scheme, coding type, number of transmitted symbols, impairments, and filter type. We then generated random transmitted symbols for the chosen modulation order and modulated the data accordingly. In the theoretical simulation, we considered three cases:

- Signal + Noise
- Signal + Noise + Crosstalk
- Signal + Crosstalk

To assess the impact of crosstalk, we considered a 4×4 unitary matrix of the same dimensions as our channel model. This matrix was added for observation purposes, as it simplifies calculations and can be directly incorporated into our mathematical model without affecting any channel properties. The inversion of the unitary matrix can be easily performed. Additionally, Additive White Gaussian Noise (AWGN) was generated. This random noise is independent and identically distributed. It is worth to note that in this scenario the channel model considered is memoryless, however in demo and experimental setup some memory is introduced. Blind algorithms utilizes tap update for the adjustment of filter coefficient by considering the previously transmitted symbol to minimize the error metric. Hence, we need certain number of taps in this case which increases in practical scenario.

The number of filter taps and Samples per Symbol (SPS) can be chosen based on specific requirements. The transmitted data was resampled for further processing, and noise and/or crosstalk were added. We then defined the type of equalizer, or combination of equalizer parameters, and assessed the convergence. For the Constant Modulus Algorithm (CMA), the average power was fixed, while for the Multi Modulus Algorithm (MMA), the number of rings and their respective power levels were defined.

The algorithm then performed the tasks outlined in Section 3.2.4, depending on the type of equalization being applied. The performance and convergence of the system were evaluated based on these parameters and the defined equalization approach.

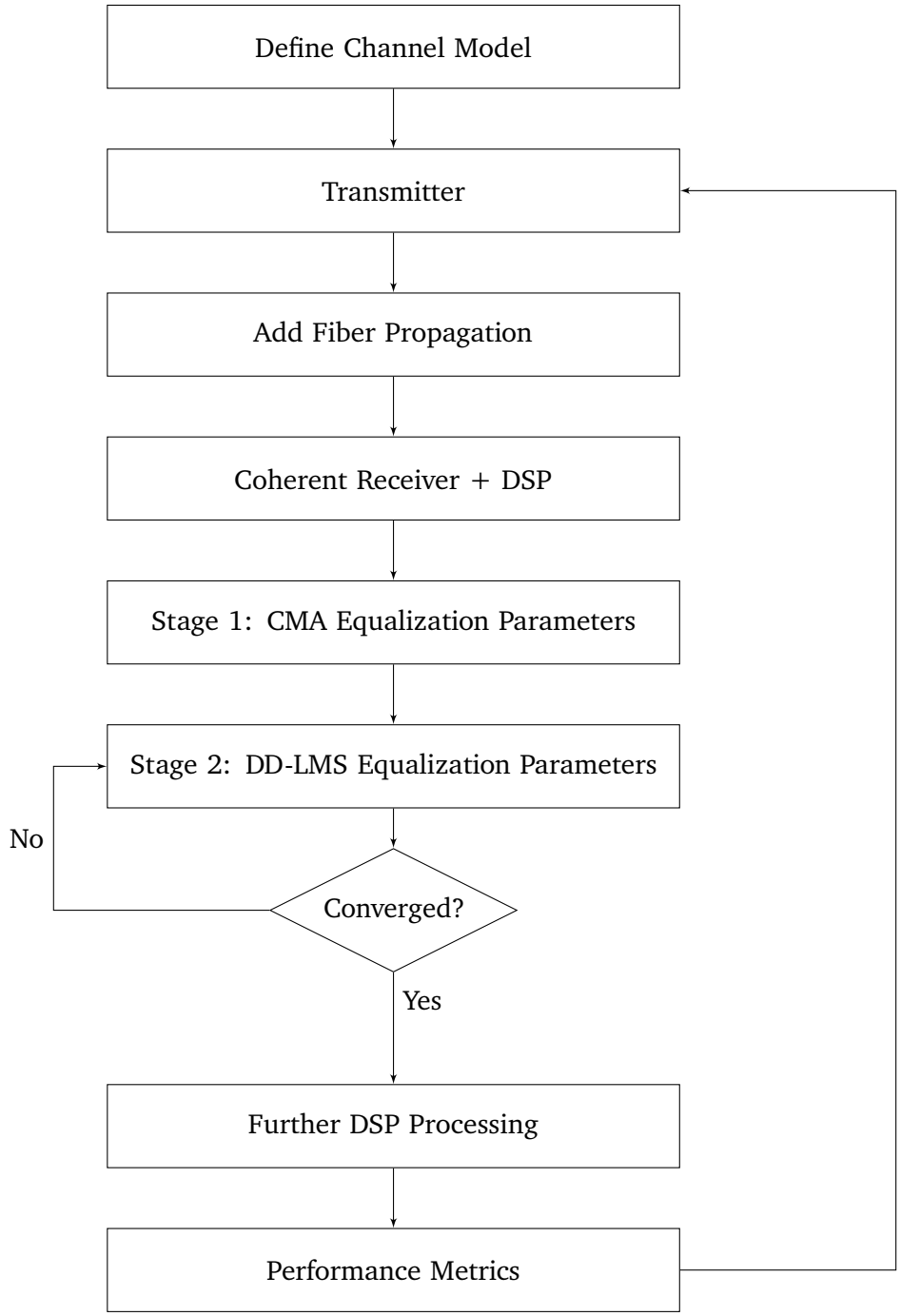

Figure 4.1: Setup and Implementation of 2-stage Adaptive Equalizers

After the Time Domain Equalization (TDE) process, the desired plots are obtained, which can be further processed. To address existing offsets, frequency offset correction and Viterbi carrier phase recovery techniques are employed. The corrected data is then sent for evaluation.

To determine the appropriate step size for the equalization algorithms, an extensive search was conducted using a brute force approach. Various combinations of the number of symbols, ranging from 2^{16} to 2^{22}, different numbers of taps, and varying iterations were tested. It was observed that a higher number of symbols resulted in better convergence and improved received constellations. Specifically, symbol numbers around 2^{19} and 2^{21} demonstrated similar performance, beyond which there was no significant improvement in the received constellation.

Interestingly, the appropriate step sizes for the Constant Modulus Algorithm (CMA), Multi Modulus Algorithm (MMA), and Decision-Directed Feed-Forward Equalization (DD-FFE) were found to be distinct from each other, despite having the same channel and initial conditions. For the chosen setup and conditions, all three algorithms yielded optimum results with step sizes within the range of 10^{-4} to 10^{-8}. Very high or very low step sizes did not yield significant enhancements or make practical sense. It is worth reiterating that the selection of an appropriate step size is crucial in determining the overall performance of the equalization algorithms. Figure 4.2 illustrates the comparison of step size selection criteria under identical conditions.

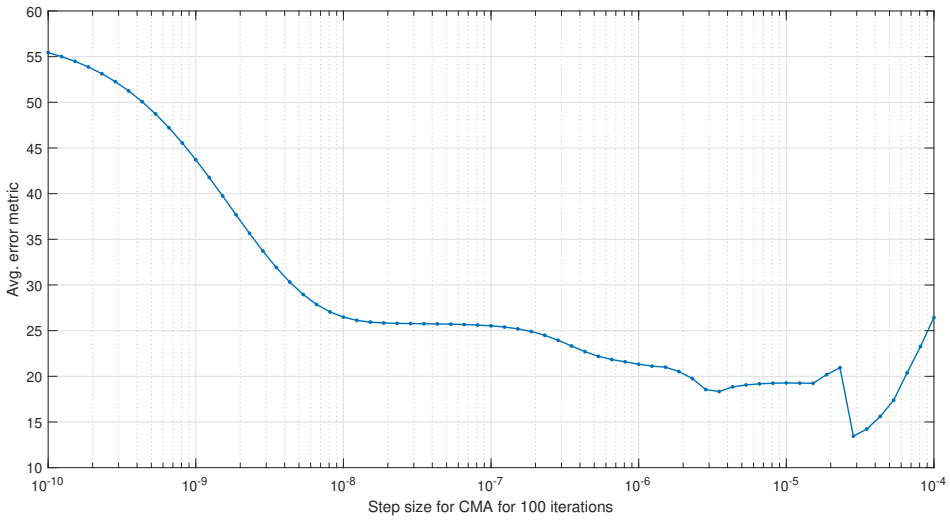

Figure 4.2: Step Size for CMA with 100 Iterations and 2^{19} Symbols

Figure 4.2 illustrates the relationship between the step size and the average error metric for 100 iterations. This simulation was conducted during the early stage of algorithm development when the equalizer was still unstable. It was observed that after a certain point, the equalizer stopped converging, and further iterations did not contribute significantly to the performance improvement. Therefore, a condition on the error was redefined, and the step size was further adjusted and tested.

In this specific figure, the Constant Modulus Algorithm (CMA) was used for QPSK modulation in the presence of noise and crosstalk. The plot indicates that the error metric reaches a minimum between step sizes of 10^{-4} and 10^{-5}. This finding suggests that the optimal step size for achieving the lowest error lies within this range.

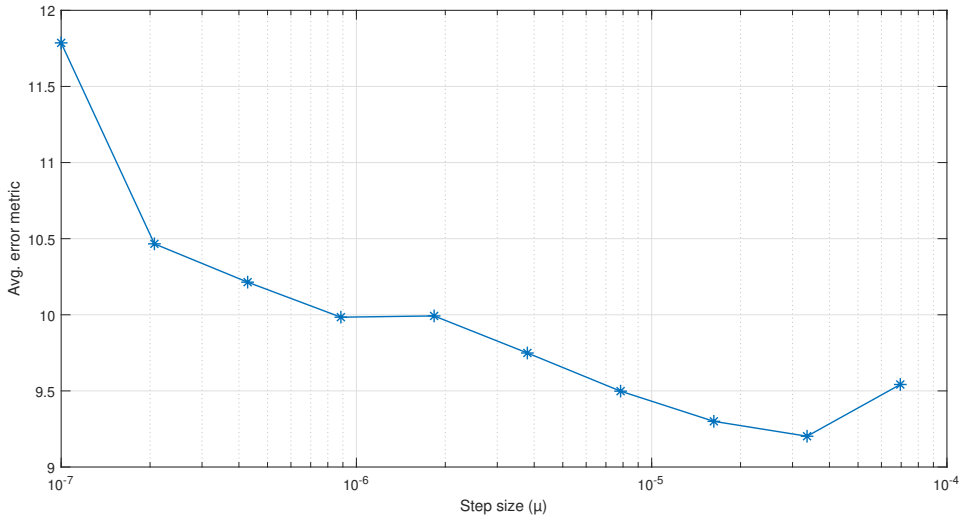

Figure 4.3: Step size for CMA for another range 100 iterations, 2^{19} symbols for 16-QAM

Figure 4.3 displays the plot of the Constant Modulus Algorithm (CMA) for 16-QAM modulation over 100 iterations, with step sizes ranging from 10^{-7} to 10^{-4}. This closer view allows for a better assessment of the step size selection. It can be observed that the minima are located near 10^{-4} and 10^{-5}, indicating that the optimal step size for achieving the lowest error lies within this range. However, it is important to note that further exhaustive search and simulation runs are required to thoroughly evaluate different step sizes and determine the most appropriate one. Figure 4.4 provides a more detailed overview compared to Figure 4.2, allowing for a closer examination of the step size performance.

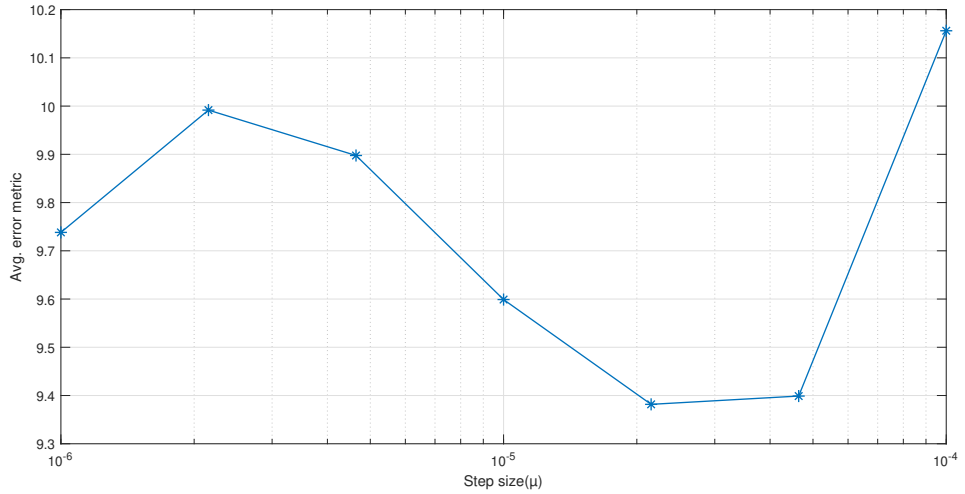

Figure 4.4: Step Size for CMA with 20 Iterations and 2^{19} Symbols (16-QAM)

Figure 4.4 presents the step size selection for 16-QAM modulation using the Constant Modulus Algorithm (CMA) in presence of noise and crosstalk. In this case, a total of 20 iterations were performed for 2^{19} symbols. The plot reveals a different behavior compared to the previous figure, but the optimum range for the step size still lies between $10^{-4} - 10^{-5}$. This indicates that the best performance in terms of error minimization can be achieved within this range of step sizes.

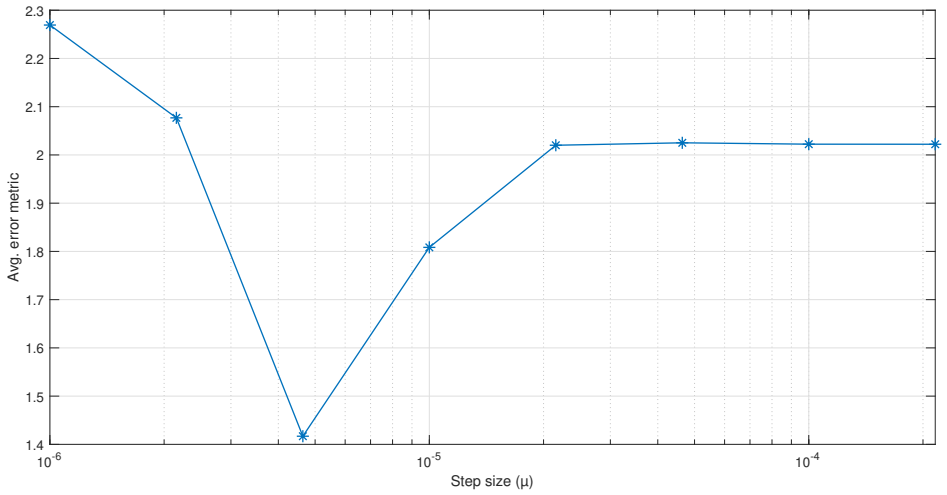

Figure 4.5: Step Size for MMA with 20 Iterations and 2^{19} Symbols (16-QAM)

Figure 4.5 illustrates the step size selection for the Multi Modulus Algorithm (MMA) applied to 16-QAM modulation. In this case, 20 iterations were performed using 2^{19} symbols. The plot demonstrates a lower average error amplitude compared to CMA, and the optimal step size is found within the range of 10^{-6} to 10^{-5}. Although the figure shows a decent behavior, further simulations are needed to obtain a closer look at the minima. These results suggest that this range is appropriate for MMA in achieving optimal performance in case of noise and crosstalk.

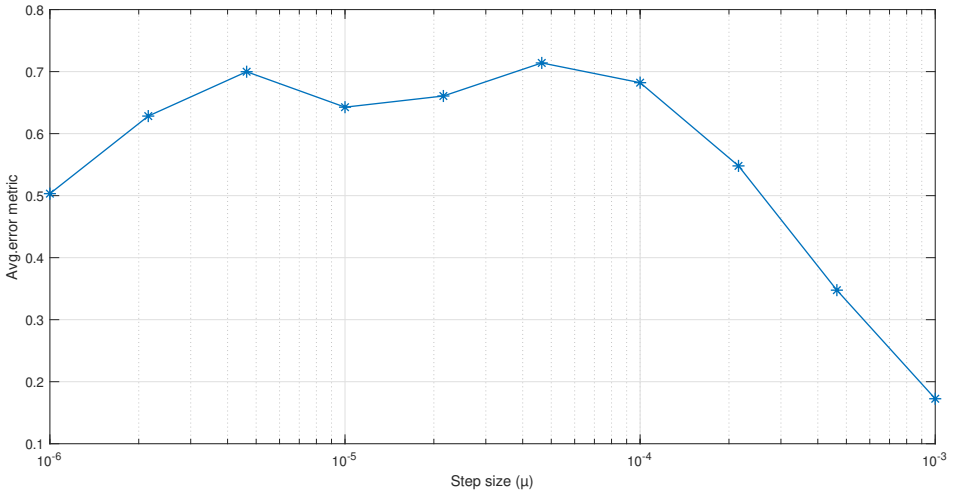

Figure 4.6: Step Size for DD-FFE 20 iterations, 2^{19} symbols, 16-QAM

Figure 4.6 depicts the step size selection for the Decision-Directed Feed-Forward Equalization (DD-FFE) which can be used in combination with CMA and MMA, in this case with MMA, using 2^{19} symbols for 16-QAM modulation. The curve adapts a slightly different pattern. In both cases, the minimum error is found within the range of 10^{-5} to 10^{-3}, which has shown promising results. The error amplitude is quite low even when the noise and crosstalk was added to this. These findings suggest that the simulated range of step size is appropriate for achieving optimal performance in DD-FFE when combined with CMA or MMA.

Table 4.1 presents the numerical values associated with the step sizes μ and error vectors for Figures 4.4 to 4.7. In some cases, the values are marked as "Inf," indicating that the algorithm stops working beyond that specific step size. Consequently, the algorithm terminates at that particular step size. It is important to note that although convergence is achieved, it does not guarantee finding global minima, as mentioned earlier. Nevertheless, these results allow for making inferences, and further assessment can be conducted to determine the appropriate step size.

μ_{vector}	$\epsilon_{vector1}$	$\epsilon_{vector2}$	$\epsilon_{vector3}$
1.00E-06	9.74E+00	2.27E+00	5.03E-01
2.15E-06	9.99E+00	2.08E+00	6.28E-01
4.64E-06	9.90E+00	1.42E+00	7.00E-01
1.00E-05	9.60E+00	1.81E+00	6.43E-01
2.15E-05	9.38E+00	2.02E+00	6.61E-01
4.64E-05	9.40E+00	2.03E+00	7.14E-01
1.00E-04	1.02E+01	2.02E+00	6.82E-01
2.15E-04	Inf	2.02E+00	5.48E-01
4.64E-04	Inf	Inf	3.48E-01
1.00E-03	Inf	Inf	1.73E-01

Table 4.1: Numerical Values of ϵ_{vector} corresponding to μ_{vector} of CMA, MMA and DD-FFE respectively, for 16-QAM, 20 iterations, 2^{19} symbols

A comparison between the step size selection of CMA and MMA in an identical scenario is depicted. The modulation scheme used was 16-QAM for 2^{19} symbols, with 20 iterations, and the presence of added noise and crosstalk. The error amplitude for CMA and MMA differs. As anticipated, CMA exhibits a higher average error amplitude and achieves the minimum at a step size of 2.1×10^{-5}. On the other hand, MMA demonstrates a significantly lower average error amplitude and attains the minimum at 4.6×10^{-6}, while also performing well at a slightly higher step size of 10^{-5}.

It is worth noting that the chosen step size varies for different scenarios and the length of the transmitted sequence. For DD-FFE, the step size was calculated in a similar manner and showed an optimum at a step size of 10^{-4}, albeit with minor variations across different cases. Consequently, when encountering slightly new scenarios, a similar step size can be selected based on the aforementioned values, which would still yield reasonable results.

4.1.2 Implementation

The error plots and received constellations were generated using Matlab code for CMA and MMA, with an additional evaluation of DD-FFE. The error plot exhibits a noisy and unstable shape, which could be attributed to the presence of offsets. The oscillating pattern observed indicates some level of convergence; however, it does not converge towards the global optimum. The lower amplitude on the y-axis signifies that the algorithm is functioning, albeit providing variable results with different iterations.

Figure 4.7 demonstrates that the constellation is significantly affected by the presence of noise and crosstalk, resulting in the loss of modulation properties. Consequently, it becomes challenging to draw meaningful inferences from such a pattern. However, adaptive blind equalization enables inference during the acquisition phase, allowing the data points to align on circular rings, which indicate different power levels. This alignment facilitates the recovery of the original information despite the adverse effects of noise and crosstalk.

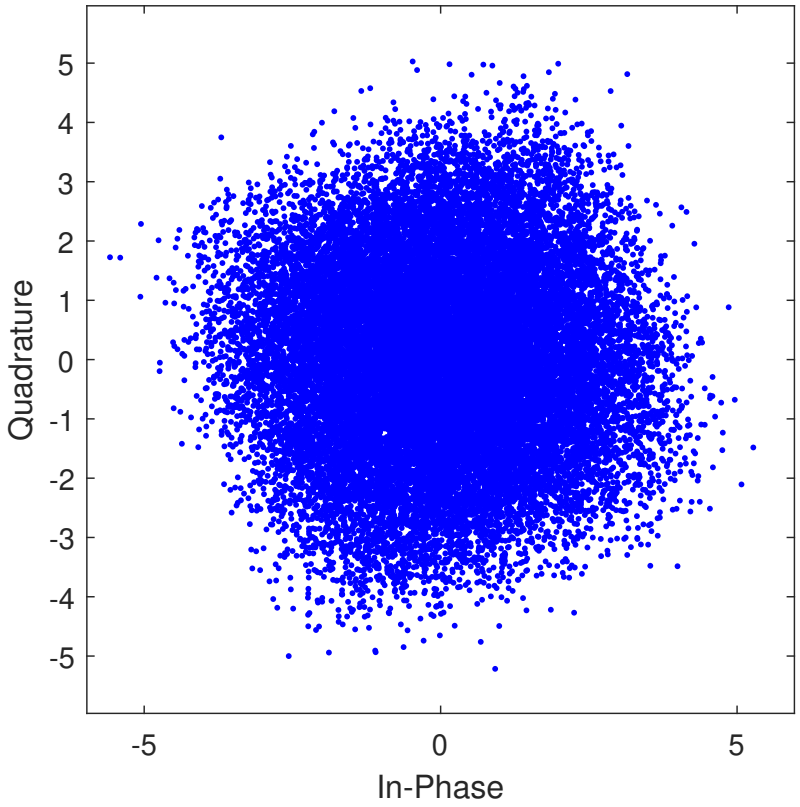

Figure 4.7: Scatterplot with Noise and Crosstalk Before Equalization

Figure 4.8 depicts the scatter plot after equalization with CMA in the presence of only noise, without the inclusion of crosstalk. The corresponding error plot is also shown. The error plot exhibits heavy oscillation; however, the error amplitude differs significantly between CMA and MMA. As anticipated, CMA performs well with QPSK modulation, resulting in a low error amplitude within the range of 0.1. The received constellation after equalization appears sharp and exhibits good quality. Figure 4.9 depicts the scatter plot for both QPSK and 16-QAM modulation schemes in a scenario similar to Figure 4.9. However, in this case, noise and

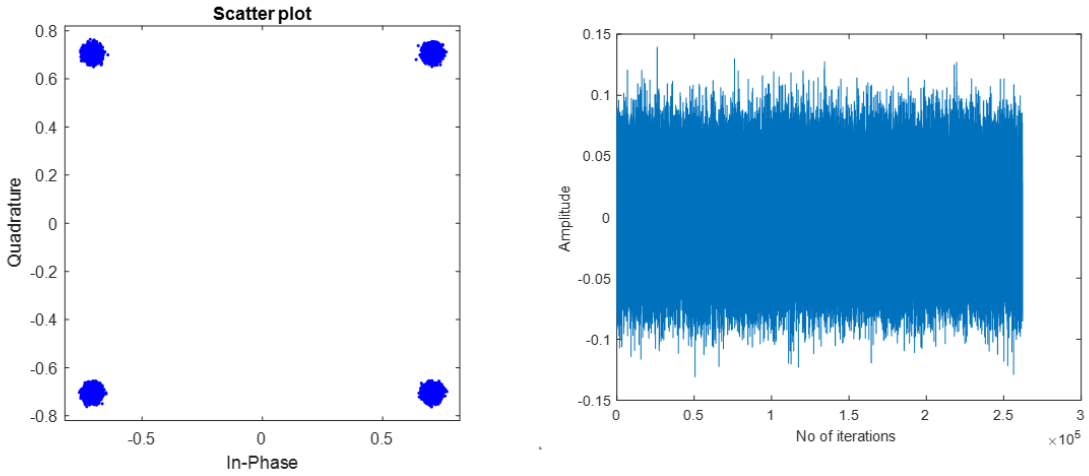

(a) Scatterplot and Error Curve for QPSK with CMA Equalization (Noise Only)

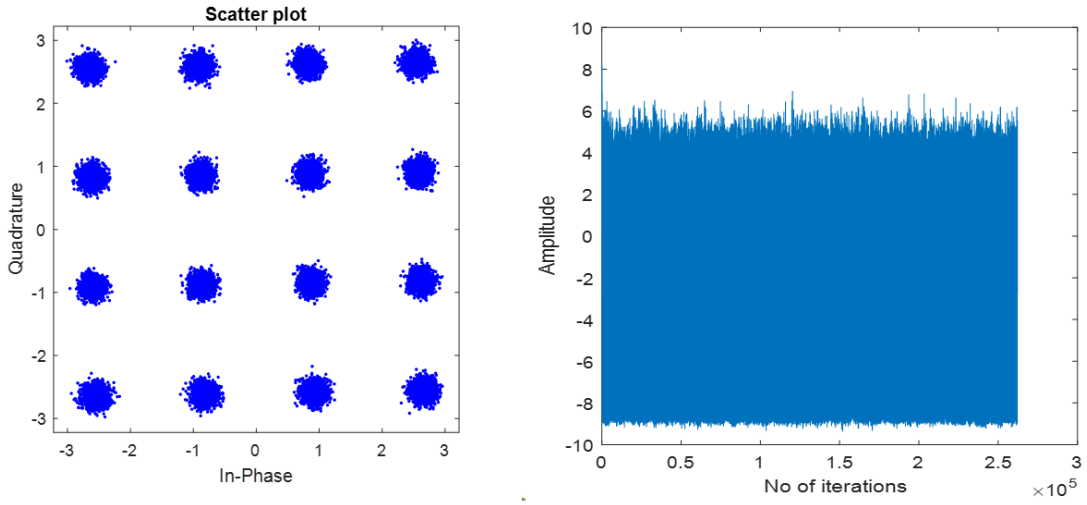

(b) Scatterplot and Error Curve for 16-QAM with CMA Equalization (Noise Only)

Figure 4.8: Results for CMA for stepsize 1e-5, only noise and no crosstalk added

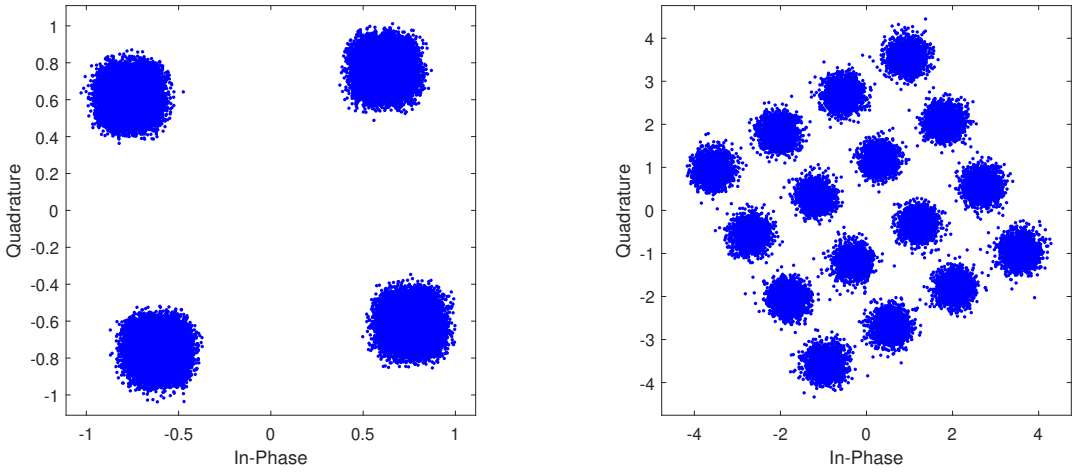

(a) Scatterplot for QPSK with CMA Equalization (Noise + Crosstalk)

(b) Scatterplot for 16-QAM with CMA Equalization (Noise + Crosstalk)

Figure 4.9: Results of CMA with 2^{19} Symbols and Step Size 2.5e-5

crosstalk are introduced. Despite these disturbances, the equalizer effectively mitigates their impact and produces satisfactory results. Notably, some data points may appear sporadic due to the number of symbols considered in the model and their misinterpretation during equalization. The rotation observed in the constellation is a consequence of phase offsets. It is important to highlight that the analysis focuses solely on evaluating the adaptive blind equalizers and does not address the phase offset in this context.

Figure 4.10 displays the results obtained using the Multi Modulus Algorithm (MMA) with a step size of 4.6e-6, which is different from the step size used in the Constant Modulus Algorithm (CMA). The constellations considered in this analysis are QPSK and 16-QAM. As expected, there is a noticeable rotation of the constellation. However, despite this rotation, the data points remain compact and do not exhibit sporadic behavior in the presence of noise. The performance of MMA is quite good even in the presence of crosstalk.

4.2 Evaluation and Performance Metrics

To assess the overall performance, effectiveness, flexibility, and adaptive extension to higher spatial dimensions of the adaptive blind equalization, it is crucial to conduct a thorough evaluation. In this chapter, we have addressed this evaluation by discussing the synthetically generated channel impairments and focusing on the convergence of the algorithms towards the optimum. Both the Constant Modulus Algorithm (CMA) and the Multi Modulus Algorithm (MMA) have demonstrated good performance during the acquisition stage, even in the presence of added crosstalk and noise. Furthermore, an extension with Decision-Directed Feed-Forward Equalization (DD-FFE) has proven to enhance the sharpness of the received constellation.

In order to evaluate the performance of the implemented blind algorithms, several well-known metrics have been defined. These metrics serve as effective measures to assess the

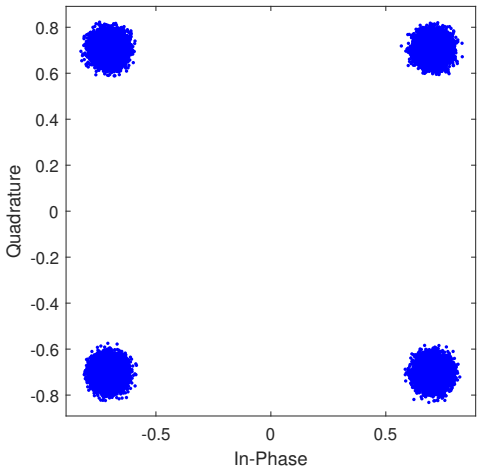

(a) Scatterplot for MMA Equalization (Noise Only)

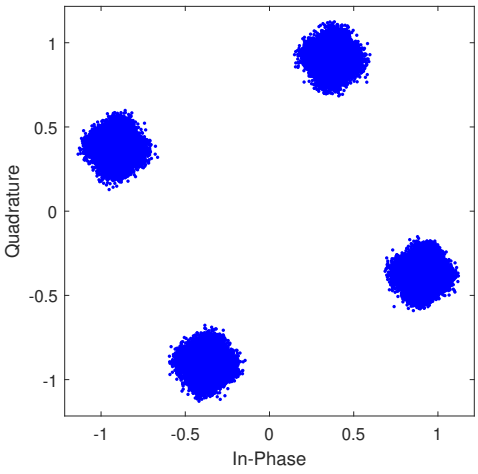

(b) Scatterplot for MMA Equalization (Noise + Crosstalk)

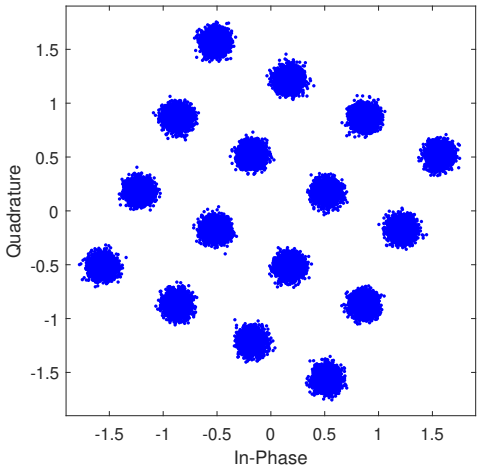

(c) Scatterplot for 16-QAM MMA Equalization (Noise Only)

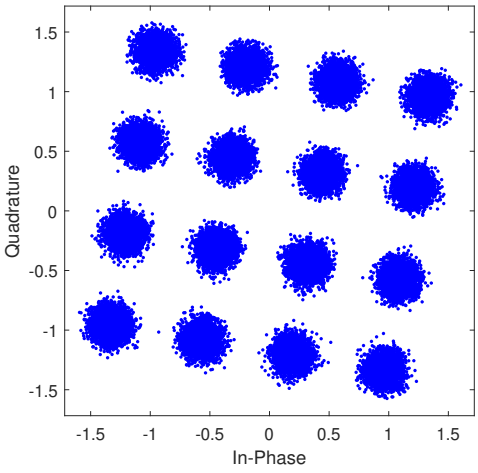

(d) Scatterplot for 16-QAM MMA Equalization (Noise + Crosstalk)

Figure 4.10: Results of MMA with 2^{19} Symbols and Step Size 4.6e-6

accuracy, quality, and signal-to-noise characteristics of the received equalized signals. The following metrics have been considered:

- **Bit Error Rate (BER):** The BER is a widely used performance metric that measures the accuracy of the received equalized signals. It quantifies the ratio of erroneous bits to the total number of transmitted bits. A lower BER indicates a more accurate estimation of the transmitted data. In the case of higher modulation orders, a higher BER is expected, which is still considered acceptable in terms of performance evaluation.
- **Error Vector Magnitude (EVM):** The EVM is a significant figure of merit for evaluating the quality of the received constellation. Since the estimator does not have knowledge of the actual transmitted data, the error vector is calculated in the Euclidean space with respect to the closest reference symbol. The EVM performs better in higher signal-to-noise ratio (SNR) regimes but may exhibit poorer performance in noisy, low SNR environments. It quantifies the root mean square error of the signal relative to the average power of the reference symbol in the constellation. The EVM is typically expressed as a percentage value, where a lower percentage indicates better performance.
- **Signal-to-Noise Ratio (SNR):** Measuring the SNR is a standard approach to assess the performance of the received signal. The SNR represents the ratio of the received signal power to the noise power and is often expressed in decibels (dB). A higher SNR is desirable for the successful decoding of the transmitted data at the receiver. However, due to various propagation effects, the SNR can degrade. It is expected that the blind algorithms perform reasonably well even in low SNR regimes. In the presence of higher noise power, additional processing may be required to obtain reliable estimates.

These metrics collectively provide valuable insights into the performance of the adaptive blind equalization algorithms, enabling an evaluation of their accuracy, constellation quality, and signal quality.

Additional metrics that are commonly considered as good standards for evaluating the performance of blind algorithms are the Q-factor and Symbol Error Rate (SER).

The Q-factor is a metric that provides an indication of the quality of the received signal by quantifying the separation between signal points in the constellation. It takes into account the effects of signal-to-noise ratio (SNR) and impairments, and it measures the overall signal quality. A higher Q-factor signifies better system performance and a lower Bit Error Rate (BER). Hence, a higher Q-factor is desirable in terms of system performance evaluation.

Symbol Error Rate (SER) is another important metric that measures the accuracy of the received symbols in a similar way to BER. It quantifies the ratio of incorrectly received symbols to the total number of transmitted symbols. SER provides insights into the robustness of the system in terms of symbol-level accuracy.

By considering these additional metrics, such as Q-factor and SER, alongside the previously mentioned BER and EVM, a comprehensive evaluation of the blind algorithms can be achieved, encompassing measures of signal quality, accuracy, and overall system performance.

5 Results of Blind Equalization

In this chapter, the results obtained from both simulations and experimental setups are presented. In the simulation setup, the generic code was enhanced and adapted by Fraunhofer which includes complete two-stage equalization with offset correction. This modified code allows for a more comprehensive analysis of multiple parameters and provides efficient results compared to the generic code. MATLAB simulations are conducted, which yield expected results with reasonable Error Vector Magnitude (EVM) and Bit Error Rate (BER) values.

Experimental results are obtained from multiple shots, but for the purpose of plotting, only the best case with the lowest average BER is presented here. A detailed analysis of all the experimental results can be found in the Appendix.

In the analysis of MIMO equalization using Digital Signal Processing (DSP), it is insightful to include the constellations, learning curve, transfer functions, and impulse response. However, for the purpose of this presentation, the transfer functions and impulse responses are demonstrated only for the simulation results to provide insights into the behavior of the filters.

By including these various analyses and results, a comprehensive understanding of the performance and behavior of the MIMO equalization scheme can be achieved.

In the obtained plots, several key parameters can be identified and analyzed:

- The constellation before the equalizer represents the unprocessed data, encompassing possible impairments such as fiber effects. This provides insight into the initial condition of the signal.
- After the first stage of equalization, the acquisition is performed using an adaptive blind equalizer for the MIMO system. However, due to the presence of offsets and other deteriorating effects, the Error Vector Magnitude (EVM) and Bit Error Rate (BER) may remain high. These effects are compensated for in later stages of the equalization process.
- The learning curve demonstrates the convergence of the step size with respect to the average error metric. It illustrates the continuous adaptation of the filter coefficients to minimize this error metric.
- The constellation with modes showcases the circular pattern observed after the first stage of equalization, with distinct points forming a modal pattern after the second stage.
- The transfer function and impulse response provide insights into the system's behavior in the presence of perturbations. They offer an understanding of how the system responds to different input signals.

- The received constellation after the second stage of equalization may still exhibit some offsets, which are further addressed and treated. This stage corrects the perturbations caused by the front end. The results after this final performance measurement are presented.

It is important to note that factors such as the phase trajectory are not discussed in this chapter, as they are addressed separately. In the experimental setup, the BER and EVM are presented for different shots, providing an understanding of the algorithm's comparative behavior in a realistic scenario. The subsequent section will delve into the simulation results.

5.1 Simulation Results

The simulation was conducted using MATLAB, although it could also be implemented using other programming languages such as C or Python. MATLAB was chosen for its existing toolbox and functions, which facilitated the processing of large datasets and execution of the desired tasks. In particular, MATLAB's 'structs' were utilized to store and process complex-sized mathematical arrays.

Various parameters were varied during the behavioral and numerical analysis. The number of bits chosen was 2^{23}, which is equivalent to 2^{19} symbols in the case of 16-QAM modulation. A samples-per-symbol ratio of 2 was set, crosstalk was added, and the linewidth was set to 100kHz. The Optical Signal-to-Noise Ratio (OSNR) was set to 21dB. A total of 4 modes were transmitted, which included the in-phase and quadrature components of $LP_{11}a$ and $LP_{11}b$.

For each of these modes, logical channels were created with a symbol rate of 32 GBaud. The bits were mapped to complex symbols. A root-raised cosine filter with a roll-off factor of 0.1 was used for pulse shaping, and the boundary behavior was set to truncation.

The equalizer parameters, such as the number of transmitters and receivers, were set to 4. The signals were normalized and resampled to 1 sample per symbol (SPS). The number of taps was set to 17, and the boundary behavior utilized cyclic extension.

For the Constant Modulus Algorithm (CMA), the step size was set to 2.5×10^{-6}. It was observed that an order of -5 did not yield the desired results compared to orders of -6 or -7. Hence, the results presented here are for a step size of order -6. For the Multi Modulus Algorithm (MMA) and Decision-Directed Least Mean Square (DD-LMS), step sizes in the range of -5 were chosen.

A window length of 500 was selected for the analysis of the learning curve adaptation cycle for 2^{19} symbols, and 200 for 2^{16} symbols. The subsequent plots are presented below.

Figure 5.1 and 5.2 illustrate the constellation before the equalizer, where the dominant presence of crosstalk and other effects is observed. The absence of a discernible pattern is evident, and the EVM is significantly high, making it difficult to distinguish individual points in the constellation. This unprocessed constellation is then passed through the first stage of the equalizer, which can be either the Constant Modulus Algorithm (CMA) or the Multi Modulus Algorithm (MMA) in this particular case.

Figure 5.3 and 5.4 depict the constellation after the first stage of equalization, with a modal representation. In these plots, circular rings can be observed, indicating the presence of different power levels within the constellation. However, these rings are still influenced

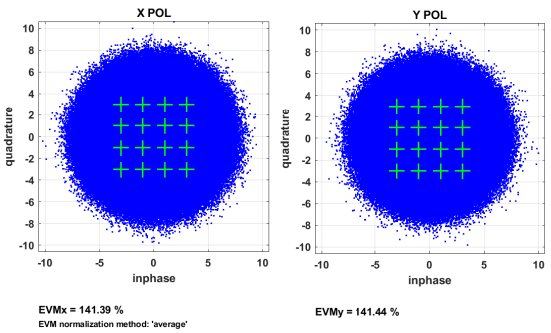

Figure 5.1: Mode 1 Before Equalizer 1

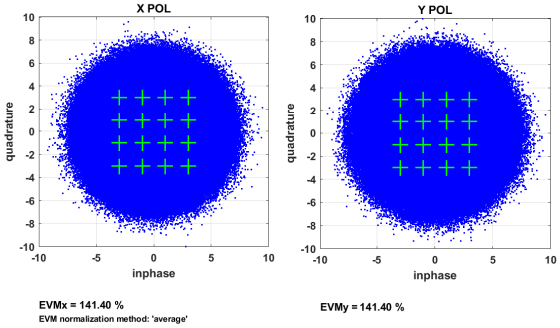

Figure 5.2: Mode 2 Before Equalizer 1

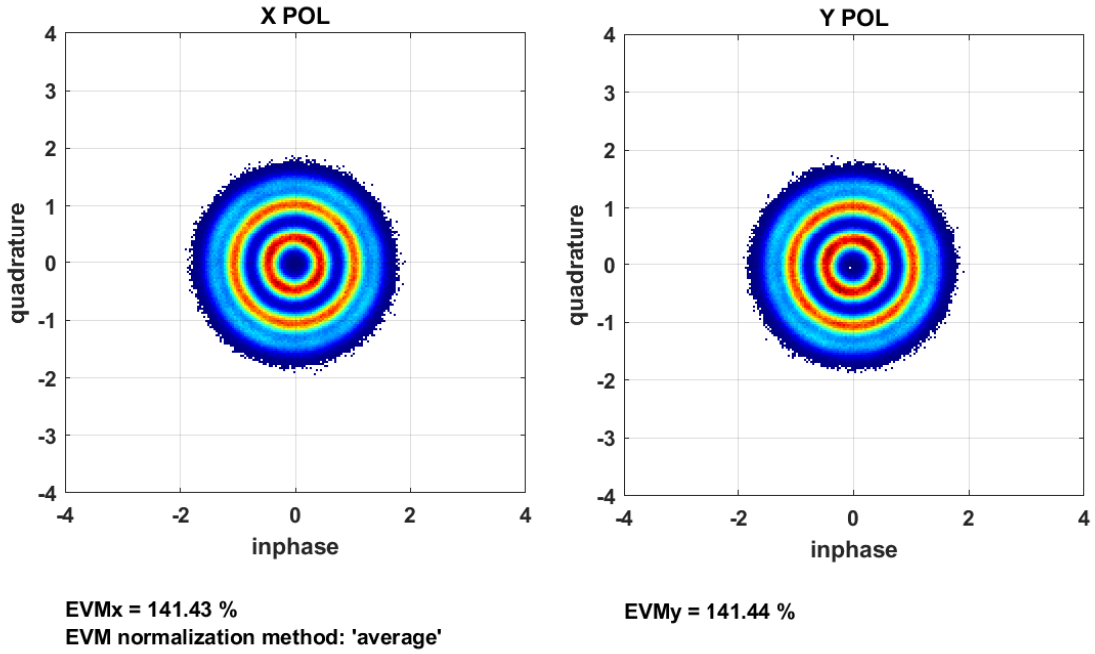

Figure 5.3: Mode 1 After Equalizer 1

by offsets, leading to a high Error Vector Magnitude (EVM). Despite this, a discernible pattern can be acquired from the constellation, suggesting some level of successful blind acquisition.

An alternative representation of Figures 5.3 and 5.4 reveals the presence of circles in the middle of the two modes, corresponding to the "Inphase" and "Quadrature" components of the "X" and "Y" polarization, respectively. Despite the heavy dominance of the noise over the constellation, it is still possible to infer certain characteristics. Even with a lower number of symbols compared to 2^{19}, distinct circles of different levels become visible which is shown in the Appendix section. Enlarging these constellations provides a better view of the circles. However, it should be noted that the high EVM is a result of the presence of offsets within the constellation.

The learning curve depicted in Figure 5.5 illustrates the adaptation cycle for 2^{19} symbols, represented as a multiple of 10^6. For a lower number of symbols, the adaptation cycle is reduced accordingly (e.g., as a multiple of 10^5). The convergence of the equalizer occurs

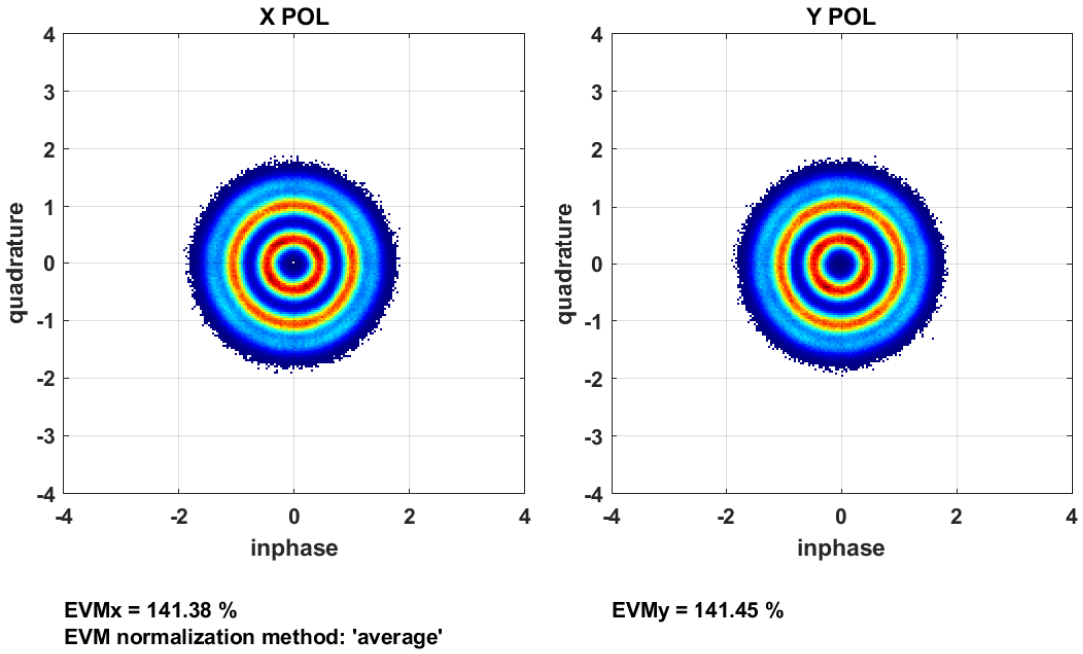

Figure 5.4: Mode 2 After Equalizer 1

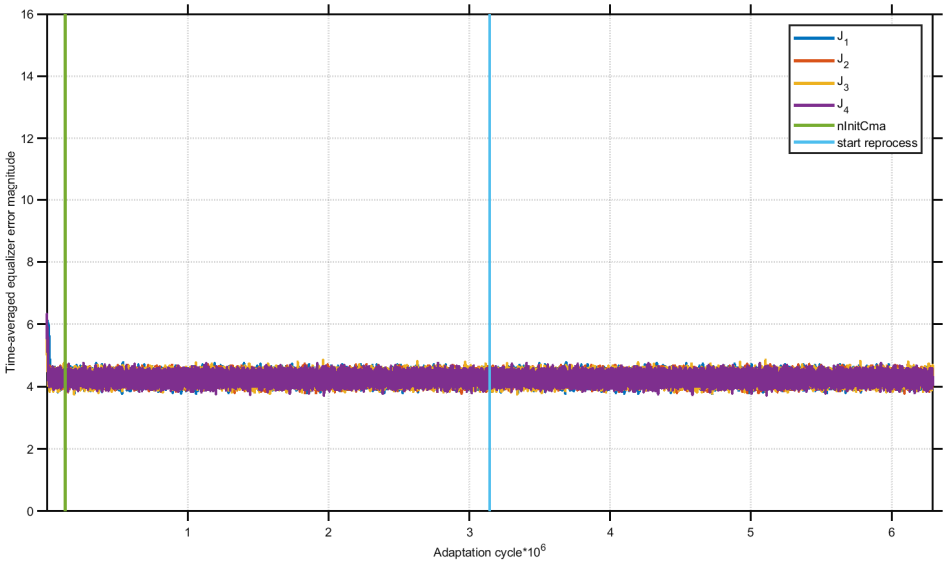

Figure 5.5: Learning Curve of Time-Averaged Equalizer Error (Window Length = 500)

before the green line, resulting in a flat response thereafter. As mentioned earlier, the learning curve demonstrates the adaptive convergence of the equalizer by updating its coefficients to minimize the error metric. This iterative process continues until the optimum value is achieved.

Figures 5.6 and 5.7 present the received constellation after the second stage of equalization, which includes frequency and phase offset correction, normalization, and frame synchroniza-

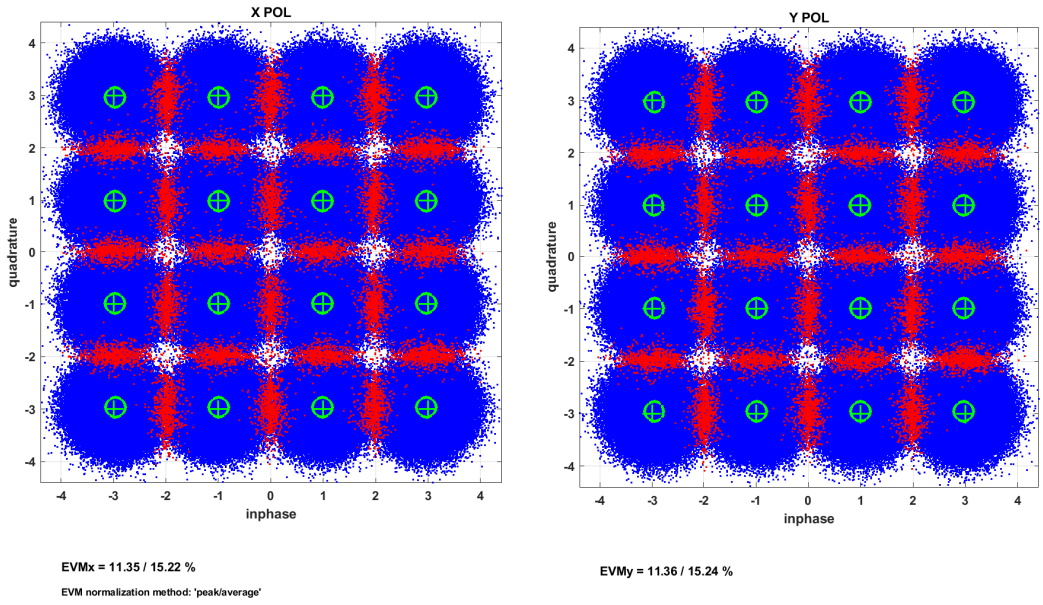

Figure 5.6: Mode 1 After Equalizer 2 and Further Processing

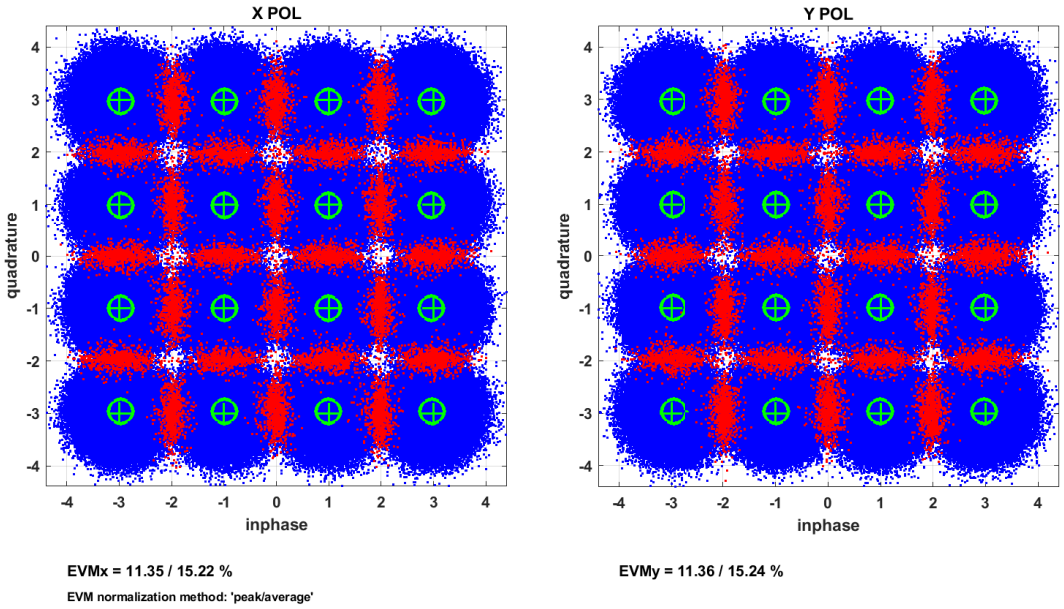

Figure 5.7: Mode 2 After Equalizer 2 and Further Processing

tion. The Error Vector Magnitude (EVM) values are shown, calculated in percentage (%), and are normalized using either the "Peak" or "Average" method. The "Peak" normalization is relative to the peak constellation power, while the "Average" method is relative to the average constellation power.

The figures display different colors for visual interpretation of correctly and falsely recovered points. The turquoise-colored circle in the middle represents the center of gravity. The center of gravity is calculated for each received point, and signals closer to it are considered to be correctly decoded bits. The color blue represents the correctly detected bits, while the red color indicates false bits lying on the border. In cases where the space is tightly closed with a higher number of bits, the appearance of red color is more noticeable.

It is important to note that relying solely on EVM for performance measurement may not be sufficient, as it can yield false results when the noise power dominates. The average Bit Error Rate (BER) in this case was reasonably close to 1.45×10^{-3}. Therefore, it can be concluded that the algorithm performed well in the presence of crosstalk and offsets.

This leads us to the next section, where the results obtained from the experimental setup are discussed.

5.2 Experimental Results

In this section, the results obtained from the experimental setup are presented. Two cases are considered: the back-to-back case without any fiber, and the case with Few Mode Fiber (FMF) of length 1 km in the lab setup are present. The back-to-back case serves as a reference for performance comparison in the presence of FMF, taking into account crosstalk and other propagation effects.

The experimental setup utilizes a 4×4 Multiple-Input Multiple-Output (MIMO) system for PDM-16QAM modulation at a symbol rate of 32 GBaud, operating in the C-band at a wavelength of 1550 nm. The linewidth is set to 100 kHz. A Digital-to-Analog Converter (DAC) and an external cavity laser (ECL) modulator are used in the setup. The channel includes a root-raised cosine filter with a roll-off factor of 0.1 for pulse shaping. The overall setup is similar to the one explained earlier.

For the FMF case, the bit-to-symbol mapping and transmission are performed over two degenerate modes of a 1 km FMF[12]. The data is split and inserted with a decorrelated delay before the first degenerate mode, and similarly for the second degenerate mode. The output signals from these two modes are received at the Coherent Receiver Frontend (CRF) and mixed with a local oscillator. The output of the CRF is then digitized using an Analog-to-Digital Converter (ADC) operating at a sampling rate of 100 GS/s. These samples are processed offline using a Digital Signal Processing (DSP) unit, as illustrated in Figure 2.1.

In the back-to-back case, the FMF is not inserted in between, resulting in the absence of crosstalk caused by the fiber. However, some polarization rotation and offsets are expected to be present. The setup is similar to the previous case, with the only difference being the absence of multi-mode transmission using FMF.

5.2.1 Back-to-Back Results

In the back-to-back case, better performance is expected due to the absence of crosstalk and fiber losses. As shown in Figures 5.8 and 5.9, the constellation after the acquisition process from the first equalizer is displayed. The constellation before the equalizer appears similar

to Figures 5.1 and 5.2, but with different Error Vector Magnitude (EVM) values. In this case, the circular rings within the constellation are more visible, allowing for better inference and analysis due to the absence of fiber effects.

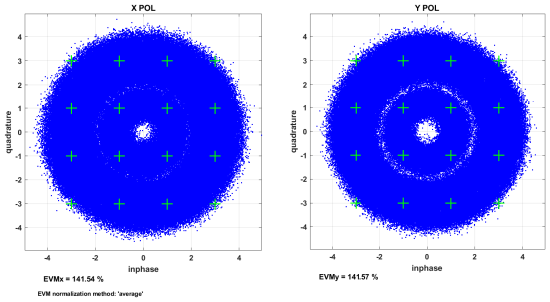

Figure 5.8: Mode 1 After Equalizer 1

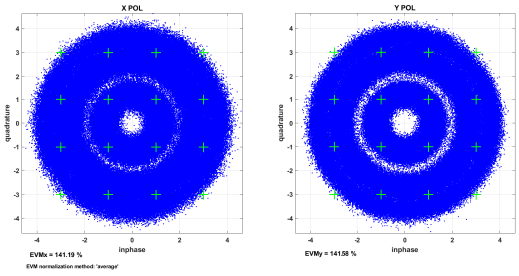

Figure 5.9: Mode 2 After Equalizer 1

In the back-to-back case, the learning curve in Figure 5.10 demonstrates the adaptation cycle with a multiple of 10^5. It is observed that the convergence occurs at a relatively higher number of iterations compared to the simulation results. However, the convergence for each coefficient is smooth, and the amplitude of the error metric is reasonable.

The parameter "nInitCma" indicates the number of symbols used for the initialization of the Constant Modulus Algorithm (CMA). Initially, it is set to false to process the samples only once after convergence is achieved. Once convergence is achieved, the processing is stopped. However, "nInitCma" is set to true again, and a portion of the samples is cropped. This step is for the deskew process using the Decision-Directed Least Mean Square (DDLMS) algorithm. The samples are reprocessed using the tap weights of the converged equalizer.

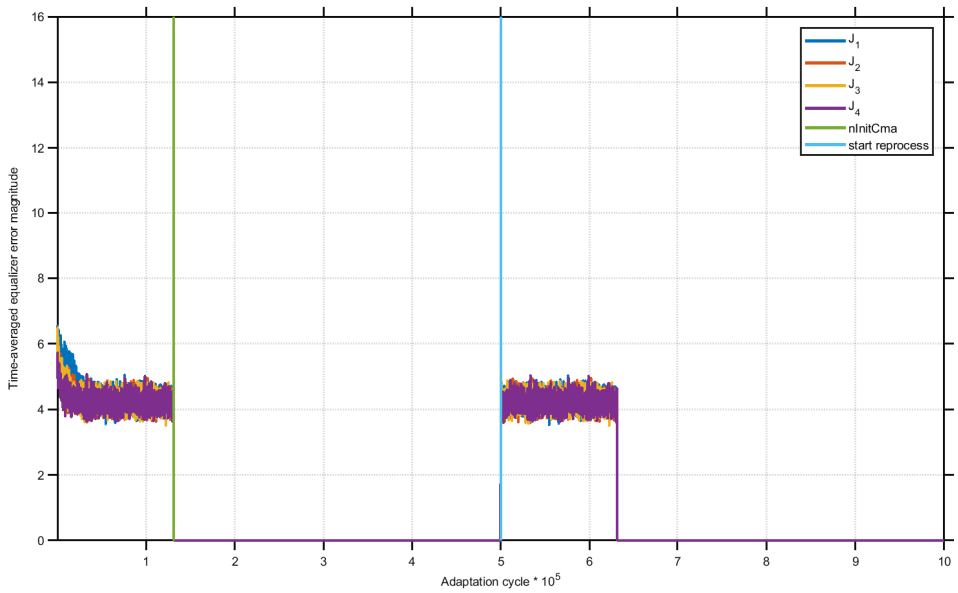

Figure 5.10: Learning Curve for Back-to-Back Case: Time-Averaged Equalizer Error (Window Length = 200)

Figures 5.11 and 5.12 display the received constellations after the second stage of equalization and additional processing. The results are quite impressive, particularly for the Y polarization in both modes. The data points appear very sharp and tightly packed towards the center of gravity, resulting in very low Error Vector Magnitude (EVM). It is highly unlikely to observe

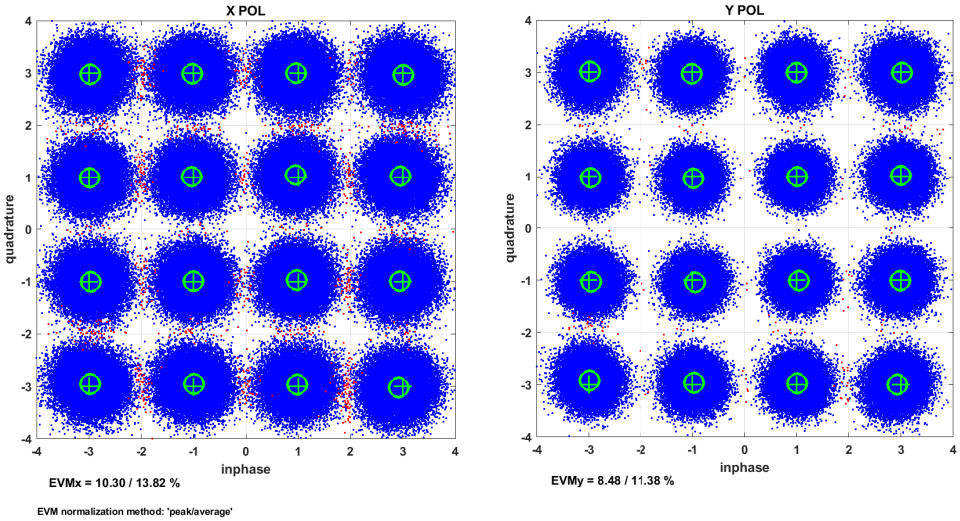

Figure 5.11: Constellation for Mode 1 After Second Equalization Stage (Back-to-Back Case)

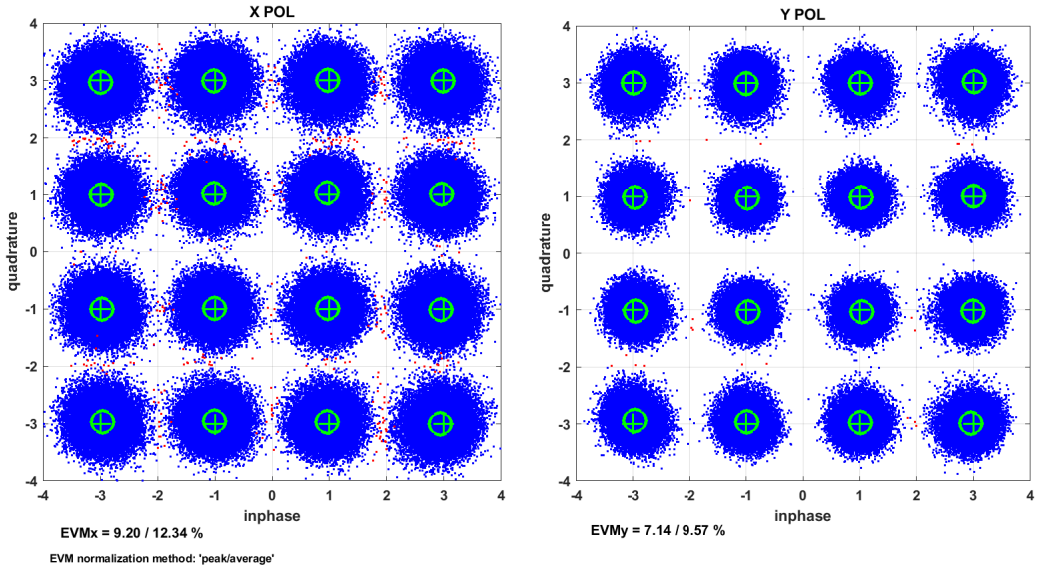

Figure 5.12: Constellation for Mode 2 After Second Equalization Stage (Back-to-Back Case)

any red points in the Y polarization, indicating a high level of accuracy in the decoding process.

However, for the X polarization, the EVM is relatively higher, with thicker circles observed away from the center of gravity. The appearance of red points is slightly more frequent in this polarization. This discrepancy could be attributed to factors such as misalignment of the polarizer or the presence of offsets. Theoretically, both polarizations should exhibit the same constellation properties.

The Bit Error Rate (BER) in this case was 1.16×10^{-4}, further indicating a satisfactory performance of the overall processing.

5.2.2 Results with Few Mode Fiber (FMF)

In the presence of Few Mode Fibers (FMF), additional effects such as crosstalk can deteriorate the overall performance. To assess the impact of these effects, Figures 5.13 and 5.14 illustrate the received constellations after the first stage of equalization. Although the circular rings may not be very distinct, some inferences can still be made from the constellations. One positive aspect is that despite the presence of crosstalk, the acquisition process is successfully carried out in the experimental setup.

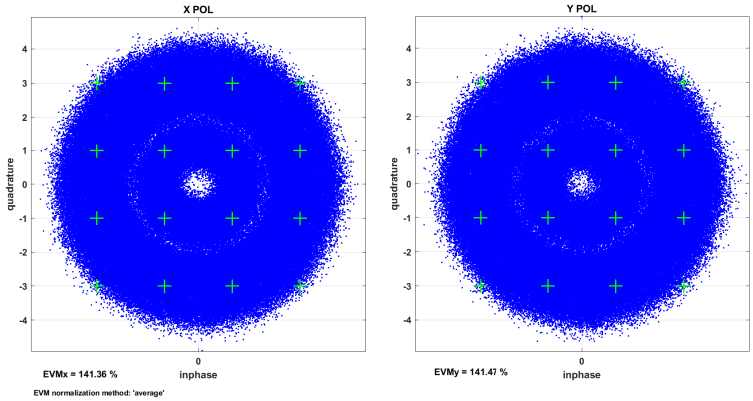

Figure 5.13: Mode 1 After Equalizer 1 for FMF Case

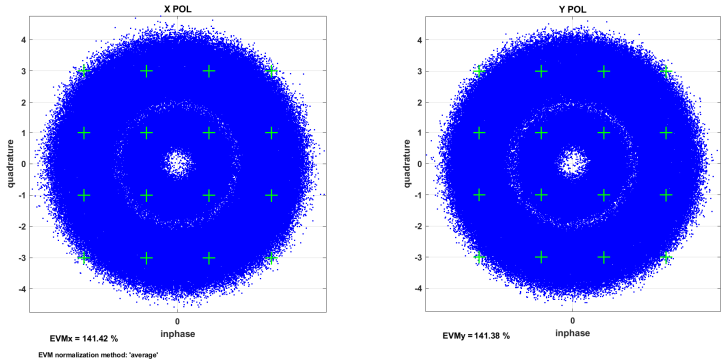

Figure 5.14: Mode 2 After Equalizer 1 for FMF Case

The learning curve in this case differs significantly from the previous cases. As depicted in Figure 5.15, the adaptation cycle is represented as a multiple of 10^5. The conditions, such as the number of symbols and the number of initialization bits, are similar to the back-to-back case. However, the curve demonstrates a comparatively poorer convergence compared to the last two cases. Additionally, each coefficient exhibits a sporadic nature, and the error metric displays a slightly higher amplitude.

Despite these observations, convergence is still achieved. Initially, the convergence is set to false until the parameter nInitCma is reached. After this point, it is set to true again to reprocess the already converged tap weights of the equalizer. Subsequently, the convergence is cropped.

As anticipated, the received constellations after the DSP with additional post-processing appear to be slightly noisier. The dominance of red points is evident, and the circles appear thicker compared to the back-to-back case. Many data points deviate from the center of

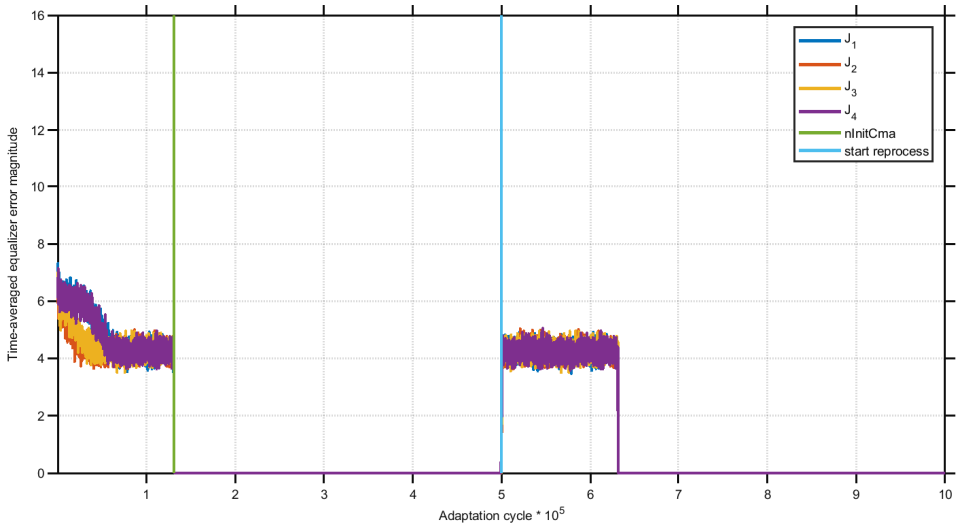

Figure 5.15: Learning Curve for Few Mode Fiber Case: Time-Averaged Equalizer Error (Window Length = 200)

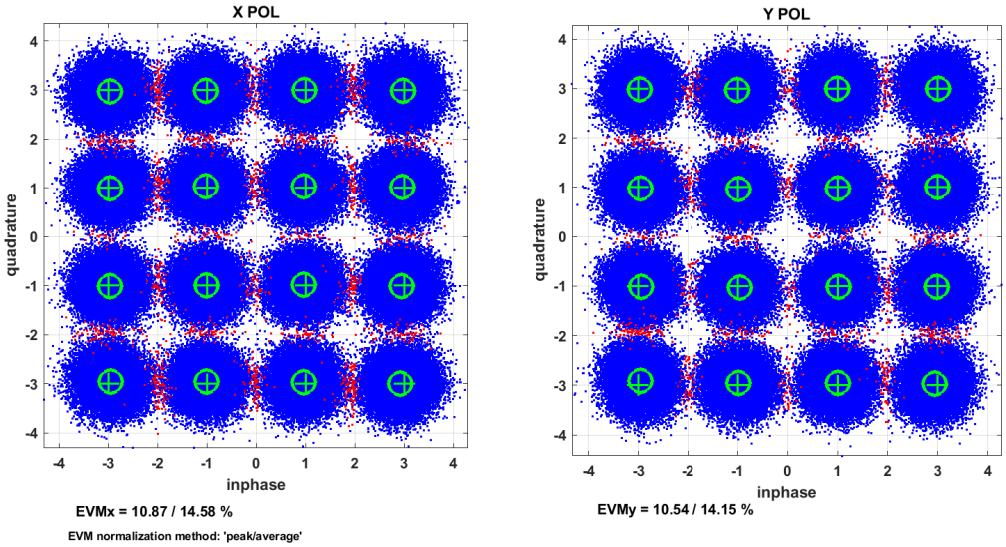

Figure 5.16: Constellation for Mode 1 After Second Equalization Stage in FMF Case

gravity, although a clear distinction can still be made easily. The error vector magnitudes (EVMs) are impressive, considering the presence of crosstalk. The low EVM of the Y polarization remains visible, indicating that some issues may be related to the experimental setup. The constellations exhibit satisfactory performance with low EVMs, although this is not consistently observed in every shot.

In this case, the average bit error rate (BER) was 5.65×10^{-4}, which is considered very good for our specific scenario. In the next section, additional factors and comparisons will be discussed.

Table 5.1 presents the results obtained from a total of four shots for both cases in the experimental setup. It includes the EVMs and BERs for both modes and both polarizations. The table demonstrates the difference between the last two back-to-back shots. Despite the lower EVM, the average BER is slightly higher for the third shot compared to the fourth shot.

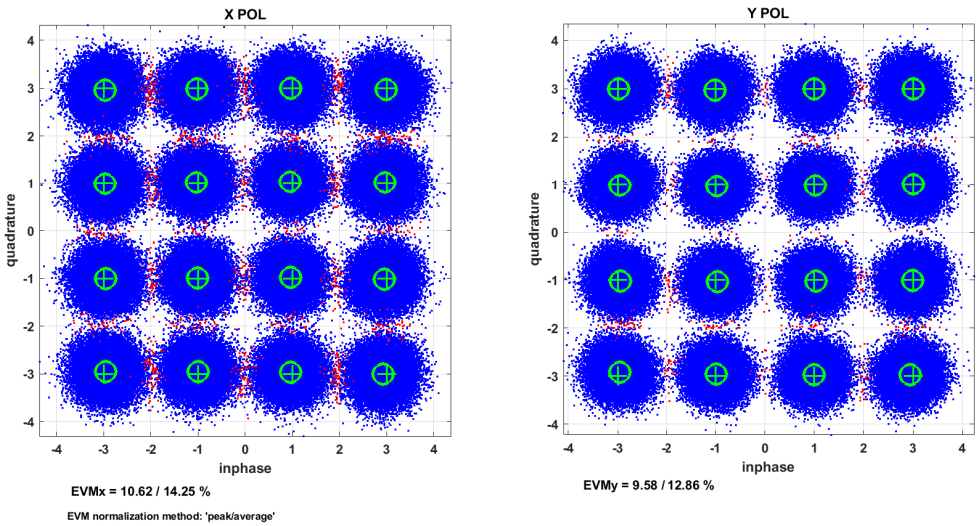

Figure 5.17: Constellation for Mode 2 After Second Equalization Stage in FMF Case

FMF or B2B	BER				EVM in %, normalization method: peak/avg				Avg BER
	Mode 1		Mode 2		Mode 1		Mode 2		
	X	Y	X	Y	X	Y	X	Y	
FMF	1.52×10^{-3}	8.5×10^{-4}	9.2×10^{-4}	3.3×10^{-4}	11.33/15.20	10.66/14.30	10.76/14.44	9.69/13.00	6.27×10^{-4}
FMF	1.02×10^{-3}	7.65×10^{-4}	8.18×10^{-4}	3.12×10^{-4}	10.87/14.58	10.54/14.15	10.62/14.25	9.58/12.86	5.65×10^{-4}
B2B	5.73×10^{-4}	6.61×10^{-5}	2.24×10^{-4}	3.07×10^{-5}	10.21/13.70	8.29/11.12	9.05/12.14	7.35/9.86	1.27×10^{-4}
B2B	5.72×10^{-4}	8.65×10^{-5}	2.16×10^{-4}	1.64×10^{-5}	10.30/13.82	8.48/11.38	9.20/12.34	7.14/9.57	1.16×10^{-4}

Table 5.1: Results for a Specific OSNR from Experimental Data

This highlights that while EVMs serve as a good figure of merit, they do not guarantee the accuracy of the system. Hence, the combination of BER and EVM is considered a credible approach for analyzing the performance.

5.2.3 Comparison of Several Parameters/Results from New Shots

For experimentation, we received multiple shots at different optical signal-to-noise ratio (OSNR) values for analysis. A total of 16 shots were processed, ranging from 16.06 dB to 45.01 dB. Due to the impracticality of plotting the constellation for each shot, this section will focus on presenting tables associated with the back-to-back and few-mode fiber cases.

In addition, EVM versus OSNR, and BER versus OSNR plots are provided for a total of four modes. As mentioned earlier, we have two LP modes and two polarizations, resulting in a total of four modes. Therefore, cumulative plots of BERs and EVMs are presented against the

OSNR levels. Additionally, the polarization of each mode was considered for BER plotting instead of the average BER. For EVM calculations, the average method was used.

1. **Back-to-back case** A total of 8 shots were taken for the back-to-back case at different OSNRs, as mentioned earlier. Figure 5.18 presents the BER versus OSNR curve, while Figure 5.19 and Figure 5.20 present the EVM versus OSNR plots. Although the BER plot appears reasonable for each mode considering the experimental setup, it does not exhibit the ideal curve. It decreases as the OSNR increases, but shows saturation at 40 dB and 45 dB instead of further BER reduction. Additionally, the BER plot behaves differently at the same OSNR for each polarization.

   The EVM curves highlight an issue associated with an outlier at 20 dB for the Y polarization of mode 2. This issue was addressed and improved by changing the initial parameter RRC (Root-raised-cosine) to the random unitary method. However, most of the shots showed better values with the RRC (Root-raised-cosine) method rather than the random unitary method.

   Table 5.2 presents all the BER and EVM values associated with each polarization and mode, along with their respective OSNRs.

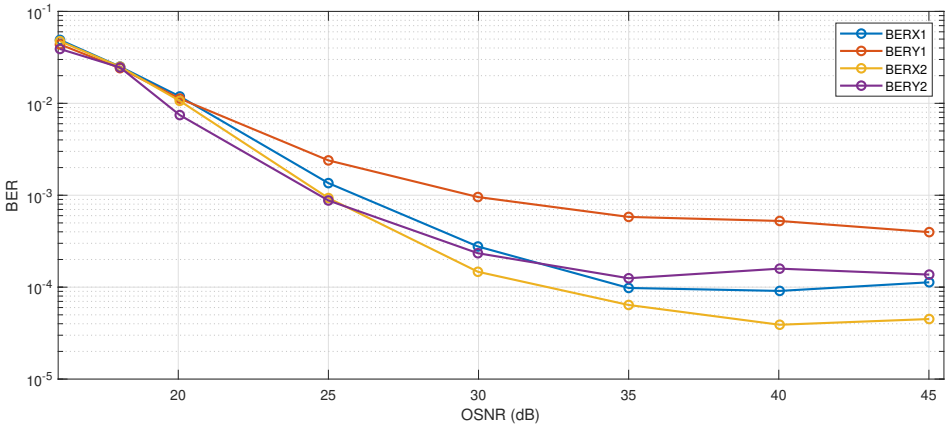

Figure 5.18: Bit Error Rate (BER) of Modes LP11a and LP11b as a Function of Optical Signal-to-Noise Ratio (OSNR) in Back-to-Back Case

2. **FMF case**

   The FMF case also includes 8 shots for the same range of OSNRs. In this section, we present the BER and EVM plots for their respective OSNRs. However, due to the reported weird outliers of mode 2, each plot is shown separately instead of cumulatively plotting. Figure 5.21 shows that the BER of mode 1 is quite stable, while for mode 2, it exhibits significant instability. A similar behavior is observed in the EVM versus OSNR plot. Each mode is plotted separately here, mainly due to the distinct and unusual behavior of mode 2 in both X and Y polarizations. As seen in the figure, for mode 1, both X and Y polarizations display relatively stable behavior.

   Table 5.3 corresponds to these BER and EVM plots and shows the faulty values of mode 2. However, this peculiar behavior is somehow altered by changing the initialization from the RRC (root-raised cosine) to the random unitary method for the receiver adaptive equalization process. Specifically, when the "Random Unitary" method was chosen and the "RRC" parameter was set to false, the performance for the same shot improved drastically. Consequently, for FMF Table 5.4, is presented, which shows comparatively improved BER and EVM values corresponding to different OSNR levels.

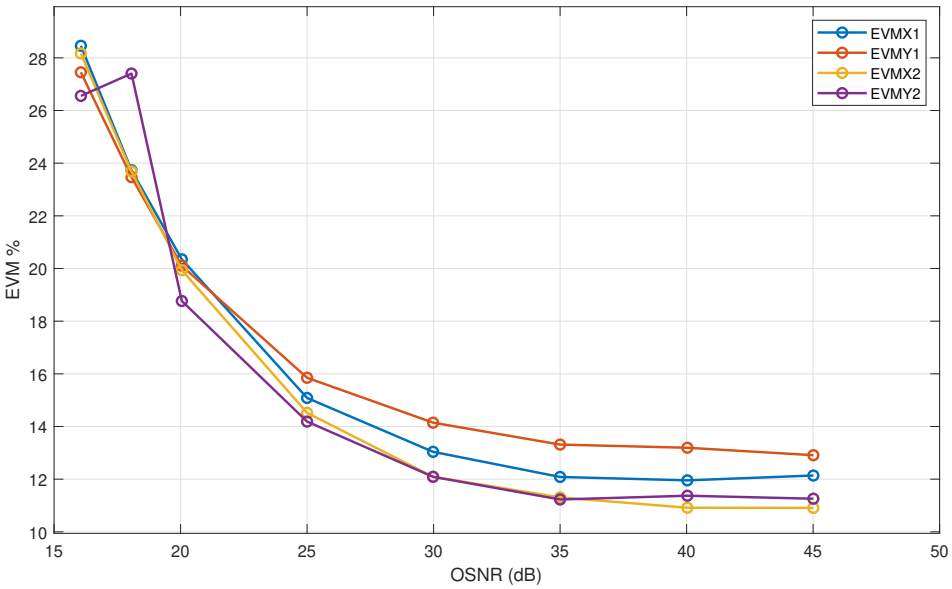

Figure 5.19: Error Vector Magnitude (EVM) of Modes LP11a and LP11b as a Function of Optical Signal-to-Noise Ratio (OSNR) in Back-to-Back Case

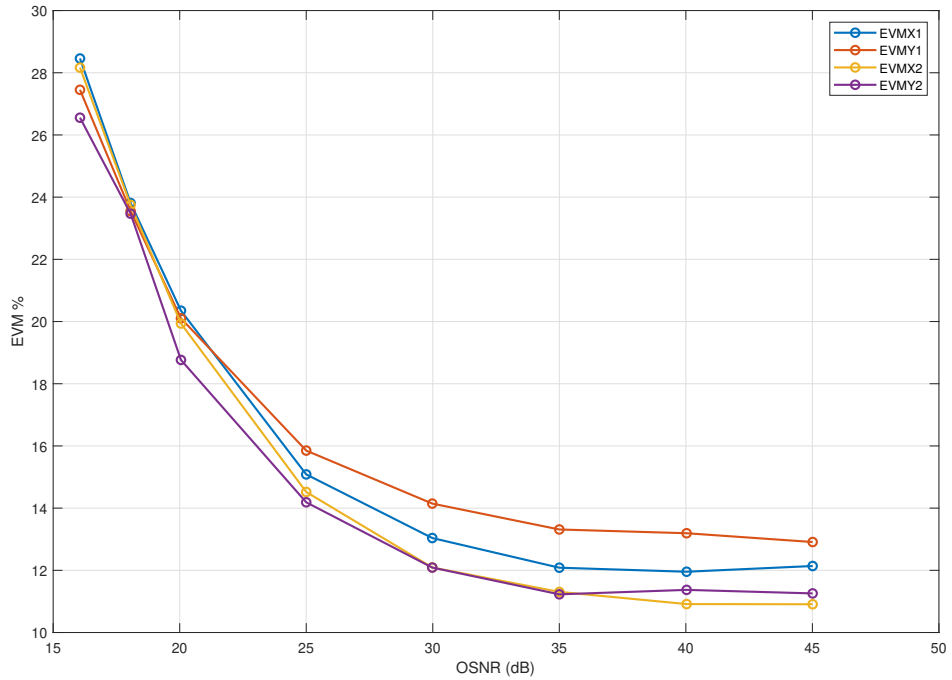

Figure 5.20: Improved Behavior: Error Vector Magnitude (EVM) of Modes LP11a and LP11b as a Function of Optical Signal-to-Noise Ratio (OSNR) in Back-to-Back Case (Including X and Y Polarization)

This table indicates a reduction in EVM and BER associated with mode 2, although we can not conclude the performance is close to the ideal curve but still decent behavior is expected. However, it is important to note that this improvement was not necessarily

OSNR(dB)	BER 1 X	BER 1 Y	BER 2 X	BER 2 Y	EVM 1 X	EVM 1 Y	EVM 2 X	EVM 2 Y
16.06	4.90×10^{-2}	4.37×10^{-2}	4.75×10^{-2}	3.90×10^{-2}	28.46	27.45	28.16	26.55
18.06	2.51×10^{-2}	2.41×10^{-2}	2.50×10^{-2}	2.46×10^{-2}	23.73	23.47	23.69	27.40
20.05	1.19×10^{-2}	1.13×10^{-2}	1.06×10^{-2}	7.45×10^{-3}	20.35	20.10	19.94	18.76
25.00	1.36×10^{-3}	2.39×10^{-3}	9.32×10^{-4}	8.77×10^{-4}	15.08	15.85	14.52	14.19
29.98	2.77×10^{-4}	9.56×10^{-4}	1.47×10^{-4}	2.34×10^{-4}	13.04	14.15	12.09	12.09
35.00	9.80×10^{-5}	5.81×10^{-4}	6.40×10^{-5}	1.25×10^{-4}	12.08	13.31	11.31	11.23
40.03	9.10×10^{-5}	5.25×10^{-4}	3.90×10^{-5}	1.59×10^{-4}	11.95	13.19	10.91	11.37
45.01	1.13×10^{-4}	3.97×10^{-4}	4.50×10^{-5}	1.37×10^{-4}	12.14	12.91	10.91	11.26

Table 5.2: BER and EVM Values for Multiple OSNR in the Back-to-Back Case

observed for all modes at distinct OSNRs, the RRC method sometimes showed better results than the random unitary method. Therefore, a separate table for the back-to-back case was not presented.

We can plot BER and EVM cumulatively for all modes in Figure 5.23 and Figure 5.24. The improved Table 5.4 utilizes RRC initialization at 16.06 dB, 30.09 dB, and 45.07 dB. The random unitary initialization did not enhance the performance metric significantly at these points for each polarization. Considering the difficulty with plotting due to the inclusion of outliers, the overall performance is improved than the previous plots; however, we can observe a sudden drop at 30 dB(RRC initialization, since the random unitary did not show much enhancement with performance metric) and an increment at 35 dB(Random unitary initialization improved numerically the BER and EVM metric of outlier, but degraded the metric of some of the X\Y polarization). Afterward, the performance exhibits a decremental trend. Considering the experimental setup with adaptive blind equalization, we can still deduce that it worked and the results demonstrate reasonable performance with some condition tweaking(in our case mainly the initialization).

There is a scope for improvement, and possibilities to manipulate more parameters or try various initialization methods with different measured datasets. For this work, two initialization methods were tried, at some OSNRs this change improved BER and EVM for the outliers but not necessarily for all polarizations. For the remaining OSNRs, the performance metric is similar to Table 5.3, as the change in initialization did not enhance overall BERs and EVMs at those specific OSNRs for all polarizations. The experimental setup can introduce unknown performance limiting factors, which need to be observed separately.

OSNR(dB)	BER 1 X	BER 1 Y	BER 2 X	BER 2 Y	EVM 1 X	EVM 1 Y	EVM 2 X	EVM 2 Y
16.06	5.16×10^{-2}	4.35×10^{-2}	4.98×10^{-2}	3.96×10^{-2}	28.93	27.40	28.56	26.68
18.06	2.76×10^{-2}	2.46×10^{-2}	4.99×10^{-1}	2.23×10^{-2}	24.27	23.58	140.29	23.14
20.04	1.37×10^{-2}	1.21×10^{-2}	4.99×10^{-1}	9.88×10^{-3}	20.87	20.43	140.87	19.67
25.00	3.97×10^{-3}	3.63×10^{-3}	4.98×10^{-1}	1.76×10^{-3}	17.10	16.83	140.45	15.35
30.09	6.73×10^{-4}	1.20×10^{-3}	5.81×10^{-4}	4.89×10^{-4}	13.97	14.78	13.78	13.35
35.04	5.19×10^{-4}	7.85×10^{-4}	1.22×10^{-3}	4.98×10^{-1}	13.58	13.94	14.84	140.57
40.02	2.23×10^{-4}	5.43×10^{-4}	4.98×10^{-1}	4.46×10^{-4}	12.67	13.53	140.39	13.20
45.07	2.26×10^{-4}	4.52×10^{-4}	1.70×10^{-4}	1.17×10^{-4}	12.67	13.30	12.29	11.61

Table 5.3: BER and EVM Values for Multiple OSNR in the FMF Case

OSNR(dB)	BER 1 X	BER 1 Y	BER 2 X	BER 2 Y	EVM 1 X	EVM 1 Y	EVM 2 X	EVM 2 Y
16.06	5.16×10^{-2}	4.35×10^{-2}	4.98×10^{-2}	3.96×10^{-2}	28.93	27.40	28.56	26.68
18.06	3.93×10^{-2}	4.34×10^{-2}	4.13×10^{-2}	3.31×10^{-2}	26.60	27.35	27.01	25.40
20.04	2.57×10^{-2}	1.86×10^{-2}	2.66×10^{-2}	2.29×10^{-2}	23.83	22.16	24.01	23.20
25.00	1.07×10^{-2}	8.35×10^{-3}	1.04×10^{-2}	7.99×10^{-3}	19.93	19.07	19.90	18.93
30.09	6.73×10^{-4}	1.20×10^{-3}	5.81×10^{-4}	4.89×10^{-4}	13.97	14.78	13.78	13.35
35.04	2.08×10^{-3}	2.39×10^{-3}	2.05×10^{-3}	9.17×10^{-4}	15.73	15.90	15.77	14.29
40.02	1.21×10^{-3}	1.76×10^{-3}	1.21×10^{-3}	4.61×10^{-4}	14.87	15.40	14.85	13.39
45.07	2.26×10^{-4}	4.52×10^{-4}	1.70×10^{-4}	1.17×10^{-4}	12.67	13.30	12.29	11.61

Table 5.4: BER and EVM Values for Multiple OSNR in the FMF Case with Improved Values

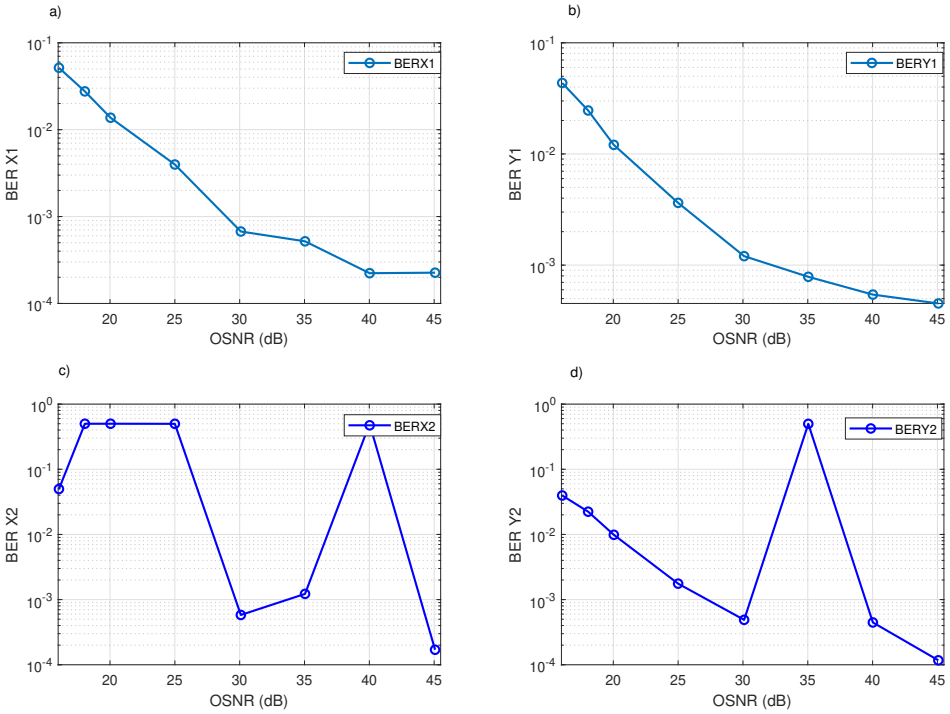

Figure 5.21: Bit Error Rate (BER) of Modes LP11a and LP11b as a Function of Optical Signal-to-Noise Ratio (OSNR) in Few Mode Fiber (FMF) Case (Including X and Y Polarization)

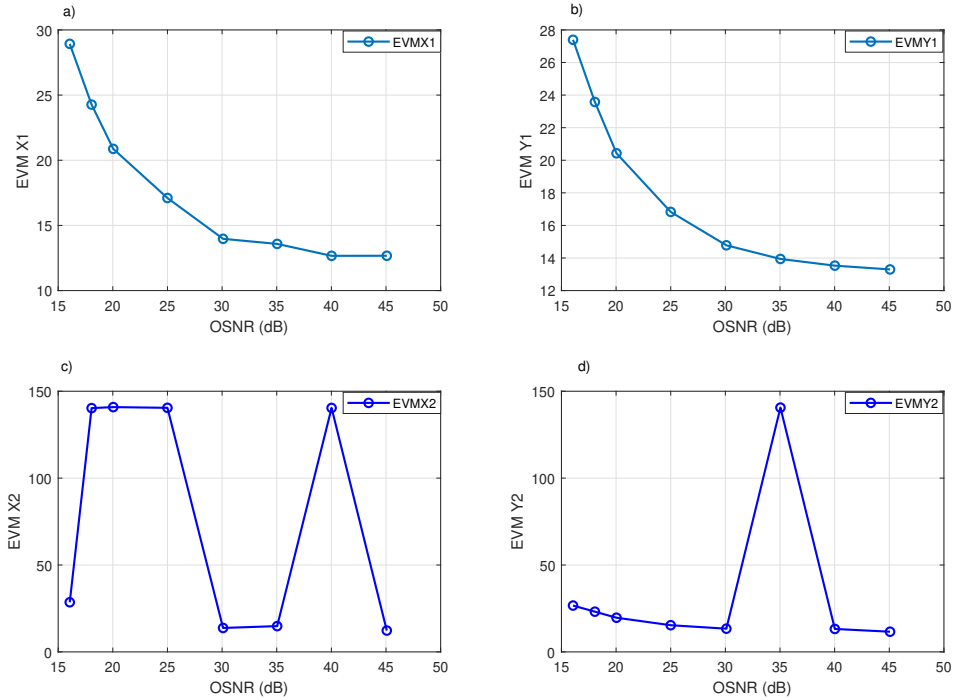

Figure 5.22: Error Vector Magnitude (EVM) of Modes LP11a and LP11b as a Function of Optical Signal-to-Noise Ratio (OSNR) in Few Mode Fiber (FMF) Case (Including X and Y Polarization)

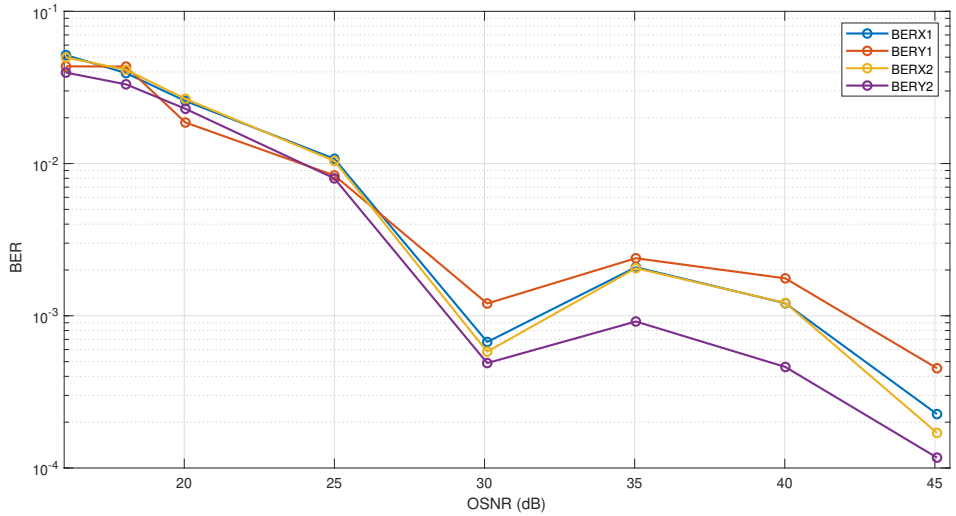

Figure 5.23: Improved BER of Modes LP11a and LP11b as a Function of Optical Signal-to-Noise Ratio (OSNR) in Few Mode Fiber (FMF) Case (Including X and Y Polarization)

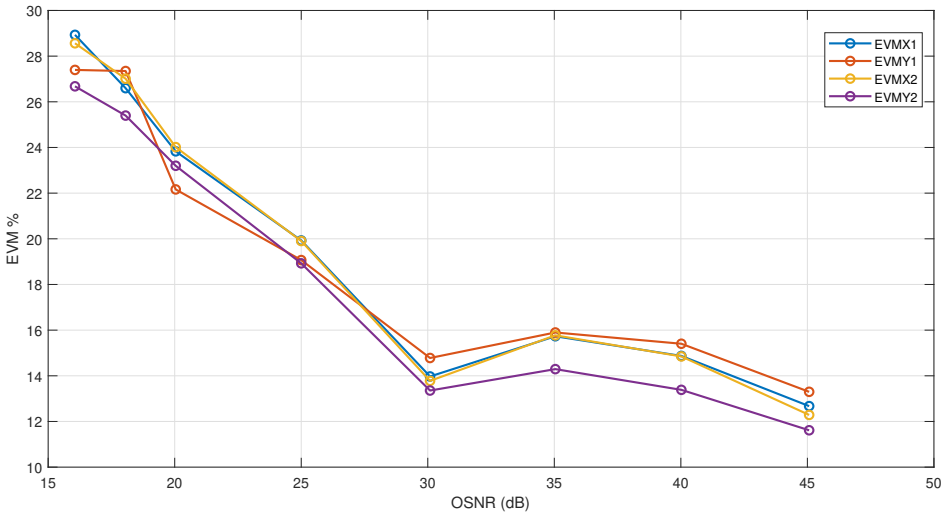

Figure 5.24: Improved EVM of Modes LP11a and LP11b as a Function of Optical Signal-to-Noise Ratio (OSNR) in Few Mode Fiber (FMF) Case (Including X and Y Polarization)

6 Conclusion

Adaptive blind equalization is a preferred approach when bandwidth constraints are a concern in high-capacity networks. This thesis has demonstrated various aspects of three popular blind algorithms, starting from the basic concepts and extending them further by incorporating DSP subsystems at the receiver in both simulation and experimental setups. The key parameters and metrics used in the evaluation indicate the adaptability of these algorithms even in diverse scenarios with added noise and crosstalk.

The next section will provide a comprehensive overview of the overall findings and discuss potential prospects in this field.

6.1 Summary

Space division multiplexing (SDM) is a promising technology that addresses the challenge of exponentially increasing data demand by enhancing network capacity through parallel pipelines. However, linear impairments and the impact of crosstalk can limit the practicality and make the realization of SDM systems a tedious task. The integration of adaptive blind equalization with coherent receivers in the DSP unit effectively addresses these issues. However, making it realizable increases the number of taps and overall system cost. Additionally, the insertion of fiber introduces dispersion and crosstalk, which are unavoidable when utilizing parallel paths within a single core with a large radius.

This thesis work highlights the implementation issues associated with Few Mode Fiber (FMF) and presents the outcomes in both simulation and experimental setups. To address the higher number of taps, an additional chromatic dispersion (CD) compensation unit utilizing static filters can be employed to compensate for most of the CD, while adaptive equalization can be used for residual CD compensation. This approach allows for the deployment of a sufficient number of taps. The adaptive blind equalizer successfully combats degradation caused by additive white Gaussian noise (AWGN) and crosstalk. The presented results validate the proof of concept and demonstrate the performance of blind equalization.

Multiple factors affect the signal recovery process, and when going blind, uncertainties associated with equalization may increase. Higher noise levels can lead to misinterpretation of false bits. The convergence of blind equalizers plays a crucial role in the successful reconstruction of transmitted symbols. Using a higher number of transmitted sequences can be an effective approach to demonstrate the effectiveness of blind equalizer convergence.

The selection of the step size is crucial and depends on the initial conditions and the considered channel model. It is important to note that the chosen step size may not be the same for all cases, as a common step size may not yield the best results. The adaptive blind equalizers may not provide optimum performance due to the lack of available information at the receiver. However, they work well when accompanied by additional units for phase and

frequency offset correction. In this case, the algorithm operates based on the magnitude of the received signal, making phase offsets unavoidable. Two-stage equalization demonstrates reasonable performance in this context.

The bit error rate (BER) of both the back-to-back and few-mode fiber cases was reasonable, and it depended on various factors as discussed in the experimental results. While the error vector magnitude (EVM) might not be the best figure of merit as it can be heavily influenced by noise in some cases, it still provides a comparative overview of the two stages of equalization and highlights the improvement associated with each stage.

It is important to note that a higher optical signal-to-noise ratio (OSNR) does not necessarily guarantee the best result, as other factors along with the impact of non-linear effects can significantly alter the overall performance. This could be also due to misalignment of the setup, lower receiver responsivity, or other component-related issues. However, adjusting the initial conditions of the equalizer can still help recover the constellation.

Furthermore, outliers associated with the modes or polarization can change the dynamics of the equalization process. However, these outliers can be limited by adjusting certain conditions of the blind equalizer. In conclusion, the overall performance of adaptive blind equalization depends on the suitable step size, initial conditions, and hardware setup and alignment in the experimental setup. Strong noise power can lead to miscalculations, but the combination of MIMO adaptive blind equalization with offset correction units and a second stage of equalization significantly improves the overall performance.

6.2 Future Work

In this work, a few-mode fiber with two modes was used for a 4x4 multiple-input multiple-output (MIMO) system employing 16-QAM modulation. However, this work can be extended to explore the performance of adaptive blind equalizers in higher numbers of modes within a few-mode fiber. As the number of modes increases, crosstalk, and modal dispersion also increase, which presents an interesting scenario to analyze the effectiveness and flexibility of the algorithm in a real-time setting.

By extending the study to higher modes in a few-mode fiber, researchers can gain valuable insights into the behavior of adaptive blind equalizers under more challenging conditions. This could help in developing robust equalization techniques that can effectively mitigate the impact of crosstalk and modal dispersion in practical scenarios.

Bibliography

[1] *Ericsson Mobility report*. https://www.ericsson.com/en/reports-and-papers/mobility-report/reports/june-2023. Accessed: 2023-08-23.

[2] *Fraunhofer HHI*. https://www.hhi.fraunhofer.de/en/news/nachrichten/2021/capacity-leap-for-fiber-optic-networks-fraunhofer-hhi-develops-real-time-signal-processing-and-qot-based-network-control-for-space-division-multiplexing. Accessed: 2023-08-23.

[3] Maxim Kuschnerov et al. "Data-Aided Versus Blind Single-Carrier Coherent Receivers". In: *Photonics Journal, IEEE* 2 (July 2010), pp. 387–403. DOI: 10.1109/JPHOT.2010.2048308.

[4] *ITU*. https://www.itu.int/hub/2023/05/space-division-multiplexing/. Accessed: 2023-08-23.

[5] *Nokia*. https://www.nokia.com/networks/optical-network-scale/. Accessed: 2023-08-23.

[6] Temitope M. Olaleye, Paulo A. Ribeiro, and Maria Raposo. "Generation of Photon Orbital Angular Momentum and Its Application in Space Division Multiplexing". In: *Photonics* 10.6 (2023). ISSN: 2304-6732. DOI: 10.3390/photonics10060664. URL: https://www.mdpi.com/2304-6732/10/6/664.

[7] Peter J Winzer and David T Neilson. "From scaling disparities to integrated parallelism: A decathlon for a decade". In: *Journal of Lightwave Technology* 35.5 (2017), pp. 1099–1115.

[8] Peter J Winzer, David T Neilson, and Andrew R Chraplyvy. "Fiber-optic transmission and networking: the previous 20 and the next 20 years". In: *Optics express* 26.18 (2018), pp. 24190–24239.

[9] René-Jean Essiambre and Robert W. Tkach. "Capacity Trends and Limits of Optical Communication Networks". In: *Proceedings of the IEEE* 100.5 (2012), pp. 1035–1055. DOI: 10.1109/JPROC.2012.2182970.

[10] Georg Rademacher et al. "1.53 Peta-bit/s C-Band Transmission in a 55-Mode Fiber". In: *2022 European Conference on Optical Communication (ECOC)*. 2022, pp. 1–4.

[11] Benjamin J. Puttnam, Georg Rademacher, and Ruben S. Luís. "Space-division multiplexing for optical fiber communications". In: *Optica* 8.9 (Sept. 2021), pp. 1186–1203. DOI: 10.1364/OPTICA.427631. URL: https://opg.optica.org/optica/abstract.cfm?URI=optica-8-9-1186.

[12] Nicolas Braig-Christophersen et al. "Experimental and Numerical Evaluation of CAZAC-type Training Sequences for MxM SDM-MIMO Channel Estimation". In: *Photonic Networks; 24th ITG-Symposium*. 2023, pp. 1–6.

[13] Kevin J. Mitchell et al. “High-speed spatial control of the intensity, phase and polarisation of vector beams using a digital micro-mirror device”. In: *Opt. Express* 24.25 (Dec. 2016), pp. 29269–29282. URL: https://opg.optica.org/oe/abstract.cfm?URI=oe-24-25-29269.

[14] John Love and Nicolas Riesen. “Mode-selective couplers for few-mode optical fiber networks”. In: *Optics letters* 37 (Oct. 2012), pp. 3990–2. DOI: 10.1364/OL.37.003990.

[15] “Recent progress in optical devices for mode division multiplex transmission system”. In: *Opto-Electronics Review* 27.3 (2019), pp. 252–267. ISSN: 1230-3402. DOI: https://doi.org/10.1016/j.opelre.2019.07.001. URL: https://www.sciencedirect.com/science/article/pii/S1230340219300472.

[16] Sercan O. Arik, Joseph M. Kahn, and Keang-Po Ho. “MIMO Signal Processing for Mode-Division Multiplexing: An overview of channel models and signal processing architectures”. In: *IEEE Signal Processing Magazine* 31.2 (2014), pp. 25–34. DOI: 10.1109/MSP.2013.2290804.

[17] Benjamin J Puttnam, Georg Rademacher, and Ruben S Luís. “Space-division multiplexing for optical fiber communications”. In: *Optica* 8.9 (2021), pp. 1186–1203.

[18] Yi Weng, Junyi Wang, and Zhongqi Pan. “Recent Advances in DSP Techniques for Mode Division Multiplexing Optical Networks with MIMO Equalization: A Review”. In: *Applied Sciences* (2019). URL: https://api.semanticscholar.org/CorpusID:117689085.

[19] Seb Savory. “Digital Coherent Optical Receivers: Algorithms and Subsystems”. In: *Selected Topics in Quantum Electronics, IEEE Journal of* 16 (Nov. 2010), pp. 1164–1179. DOI: 10.1109/JSTQE.2010.2044751.

[20] Seb J. Savory. “Digital filters for coherent optical receivers”. In: *Opt. Express* 16.2 (Jan. 2008), pp. 804–817. DOI: 10.1364/OE.16.000804. URL: https://opg.optica.org/oe/abstract.cfm?URI=oe-16-2-804.

[21] Beril Inan et al. “DSP complexity of mode-division multiplexed receivers”. In: *Optics express* 20 (May 2012), pp. 10859–69. DOI: 10.1364/OE.20.010859.

[22] Ezra Ip. “Nonlinear compensation using backpropagation for polarization-multiplexed transmission”. In: *Journal of Lightwave technology* 28.6 (2010), pp. 939–951.

[23] JP Gordon and H Kogelnik. “PMD fundamentals: Polarization mode dispersion in optical fibers”. In: *Proceedings of the National Academy of Sciences* 97.9 (2000), pp. 4541–4550.

[24] Sebastian Randel et al. “Complexity analysis of adaptive frequency-domain equalization for MIMO-SDM transmission”. In: *39th European Conference and Exhibition on Optical Communication (ECOC 2013)*. 2013, pp. 1–3. DOI: 10.1049/cp.2013.1540.

[25] Beril Inan et al. “DSP complexity of mode-division multiplexed receivers”. In: *Optics express* 20.10 (2012), pp. 10859–10869.

[26] Bernhard Spinnler. “Equalizer Design and Complexity for Digital Coherent Receivers”. In: *IEEE Journal of Selected Topics in Quantum Electronics* 16.5 (2010), pp. 1180–1192. DOI: 10.1109/JSTQE.2009.2035931.

[27] René-Jean Essiambre et al. “Capacity limits of optical fiber networks”. In: *Journal of Lightwave Technology* 28.4 (2010), pp. 662–701.

[28] Maxim Kuschnerov et al. “DSP for Coherent Single-Carrier Receivers”. In: *Journal of Lightwave Technology* 27.16 (2009), pp. 3614–3622. DOI: 10.1109/JLT.2009.2024963.

[29] David S Millar and Seb J Savory. “Blind adaptive equalization of polarization-switched QPSK modulation”. In: *Optics Express* 19.9 (2011), pp. 8533–8538.

[30] P Rajesh Kumar. “Blind Equalization using Constant Modulus Algorithm and Multi-Modulus Algorithm in WirelessCommunication Systems”. In: *International journal of computer applications* 975 (2010), p. 8887.

[31] Hadrien Louchet, Konstantin Kuzmin, and Andre Richter. “Improved DSP algorithms for coherent 16-QAM transmission”. In: *2008 34th European Conference on Optical Communication*. 2008, pp. 1–2. DOI: 10.1109/ECOC.2008.4729195.

[32] João Mendes Filho, Magno T. M. Silva, and Maria D. Miranda. “A family of algorithms for blind equalization of QAM signals”. In: *2011 IEEE International Conference on Acoustics, Speech and Signal Processing (ICASSP)*. 2011, pp. 3388–3391. DOI: 10.1109/ICASSP.2011.5947112.

[33] Michael J Ready and Richard P Gooch. “Blind equalization based on radius directed adaptation”. In: *International Conference on Acoustics, Speech, and Signal Processing*. IEEE. 1990, pp. 1699–1702.

[34] Joao Mendes Filho et al. “A region-based algorithm for blind equalization of QAM signals”. In: *2009 IEEE/SP 15th Workshop on Statistical Signal Processing*. IEEE. 2009, pp. 685–688.

[35] A Hyvärinen and Erkki Oja. “Oja, E.: Independent Component Analysis: Algorithms and Applications. Neural Networks 13(4-5), 411-430”. In: *Neural networks : the official journal of the International Neural Network Society* 13 (June 2000), pp. 411–30. DOI: 10.1016/S0893-6080(00)00026-5.

[36] Vincent Lauinger, Fred Buchali, and Laurent Schmalen. “Blind equalization and channel estimation in coherent optical communications using variational autoencoders”. In: *IEEE Journal on Selected Areas in Communications* 40.9 (2022), pp. 2529–2539.

[37] Chaoran Huang et al. “High-Capacity Space-Division Multiplexing Communications With Silicon Photonic Blind Source Separation”. In: *Journal of Lightwave Technology* 40.6 (2022), pp. 1617–1632. DOI: 10.1109/JLT.2022.3152027.

[38] Xiang Liu et al. “Demonstration of 144-Gbps Photonics-Assisted THz Wireless Transmission at 500 GHz Enabled by Joint DBN Equalizer”. In: *Micromachines* 13.10 (Sept. 2022), p. 1617. ISSN: 2072-666X. DOI: 10.3390/mi13101617. URL: http://dx.doi.org/10.3390/mi13101617.

A Interpreting Experimental Results

Back-to-Back results for 2^{16} symbols

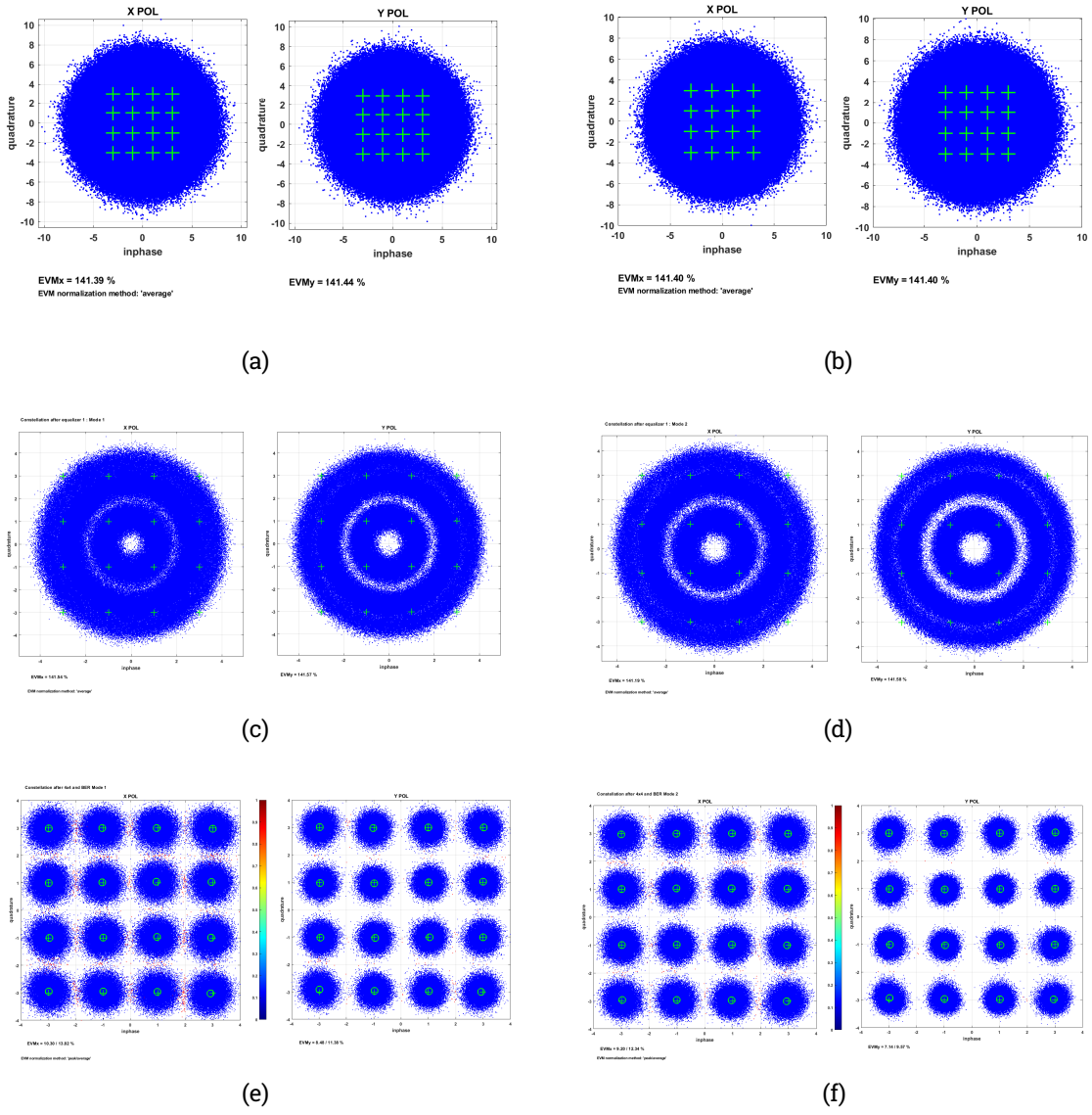

(a) (b)

(c) (d)

(e) (f)

Figure A.1: Constellations before and after 2 stage equalization

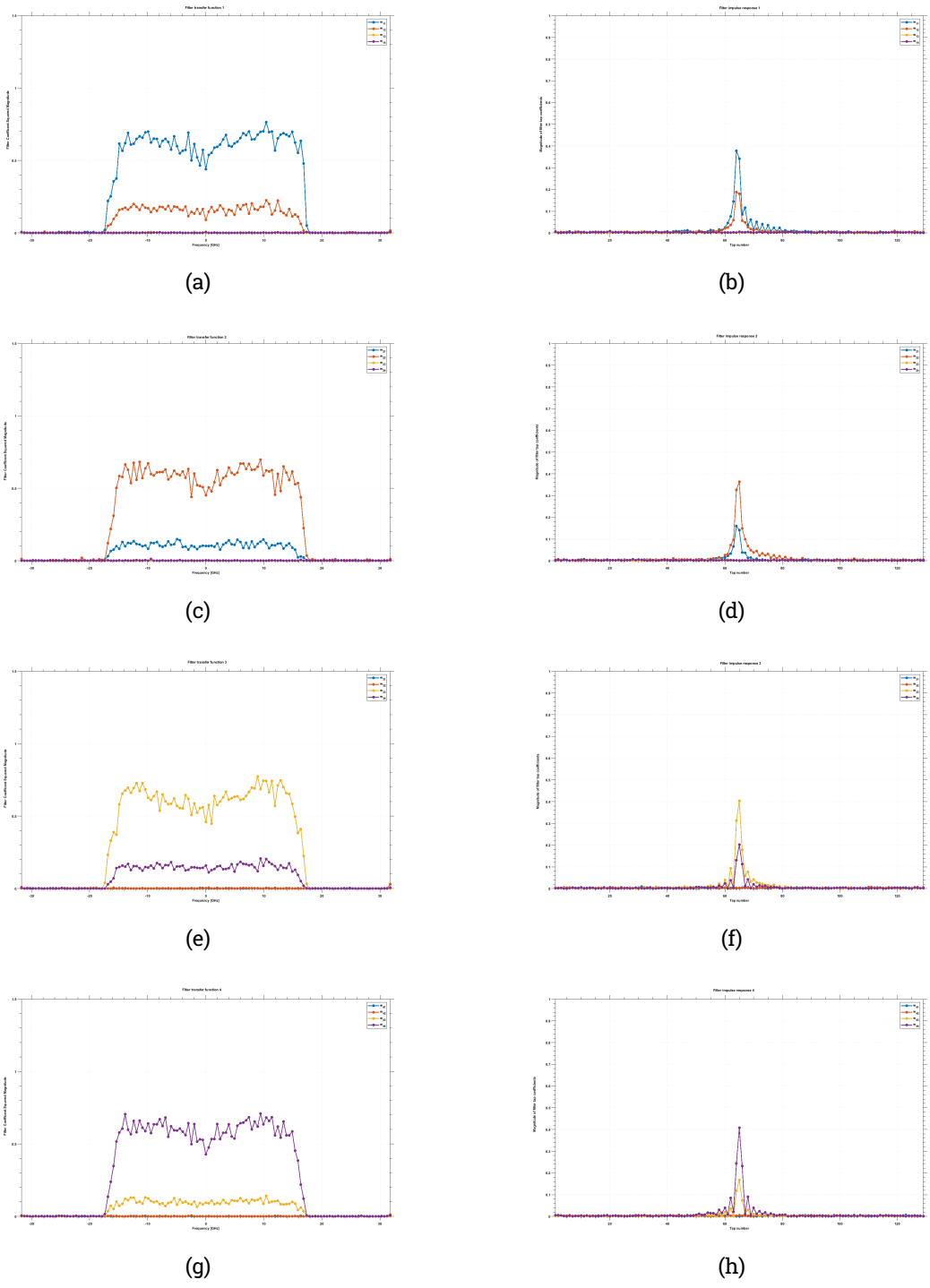

(a) (b) (c) (d) (e) (f) (g) (h)

Figure A.2: Transfer function with corresponding impulse response

B Choosing the Right Step Size

The selection of the correct step size is a tedious task, and it is important to ensure its accuracy. Figure B.1 provides a comprehensive overview of all four scenarios. However, relying solely on the results depicted in the figure might be misleading. Therefore, simulations were conducted to validate the accuracy of the desired step size.

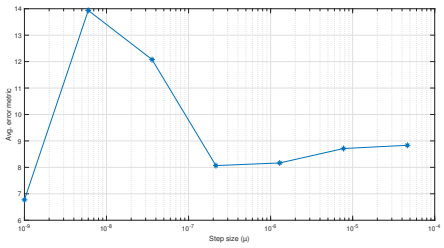

(a) Step size for CMA for 20 iterations

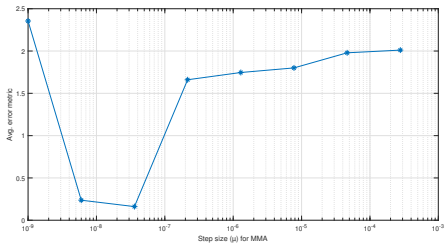

(b) Step size for MMA for 20 iterations

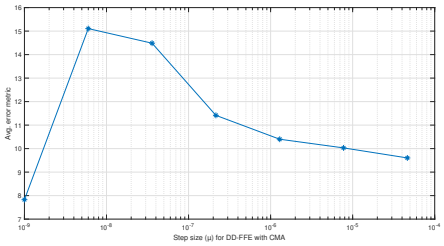

(c) Step size for DD-FFE with CMA for 20 iterations

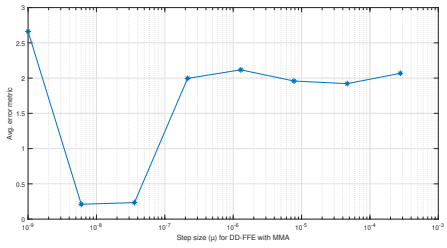

(d) Step size for DD-FFE with MMA for 20 iterations

Figure B.1: Step size selection for all three algorithms for 20 iterations and 2^{19} symbols

μ_{vector}	ϵ_{vector}			
	CMA	CMA + DD-LMS	MMA	MMA + DD-LMS
1.000e-09	6.773	7.827	2.355	2.661
5.995e-09	1.394e+01	1.511e+01	2.367e-01	2.108e-01
3.594e-08	1.208e+01	1.448e+01	1.613e-01	2.342e-01
2.154e-07	8.067	1.141e+01	1.661	1.996
1.292e-06	8.167	1.040e+01	1.746	2.117
7.743e-06	8.712	1.003e+01	1.801	1.959
4.642e-05	8.834	9.603	1.979	1.921
2.783e-04	Inf	Inf	2.011	2.068
1.668e-03	Inf	Inf	Inf	Inf
1.000e-02	Inf	Inf	Inf	Inf

Table B.1: Numerical Values of ϵ_{vector} corresponding to μ_{vector} for 16-QAM, 20 iterations, 2^{19} symbols

Abbreviations

MIMO	Multiple-Input and Multiple-Output
SDM	Space division multiplexing
WDM	Wavelength division multiplexing
QPSK	Quadrature Phase Shift Keying
SPS	Samples per symbol
N	Received signal length
M	Transmitted signal length
yLength	Length of the discrete-time dimension of $\mathbf{y}_{N\times 1}$ and $\mathbf{z}_{N\times 1}$
xLength	Length of the discrete-time dimension of $\mathbf{x}_{M\times 1}$
hLength	Length of the discrete-time dimension of $\mathbf{H}_{N\times M}$
wLength	Number of taps of the equalizer filter (or length of the discrete-time dimension of $\mathbf{W}_{}$
$\hat{\mathbf{x}}_{m\times 1}$	Equalizer output

$\tilde{\mathbf{y}}^p[n]$	pth batch of vector $\mathbf{y}[n]$
$\hat{\mathbf{x}}^p[m]$	$\hat{\mathbf{x}}$ at discrete time instant p
$\mathbf{W}^j[m,n]$	jth iteration of $\mathbf{W}[m,n]$
ϵ_m	Error
ϵ_m^j	jth iteration of the error
PMD	Polarization mode dispersion
RRC	Root-raised-cosine
CD	Chromatic dispersion
AWGN	Additive white Gaussian noise
FMF	Few Mode Fiber
EVM	Error vector magnitude
BER	Bit error rate
OSNR	Optical signal-to-noise ratio
MMF	Multimode fibers
SMF	Single-mode fibers

List of Figures

List of Tables